12-1-2010

Autonomous Wireless Radar Sensor Mote for Target Material Classification

Muhammad Mahmudur Rahman Khan

To the University Council:

The Thesis Committee for Muhammad Mahmudur Rahman Khan certifies that this is the final approved version of the following electronic thesis: "Autonomous Wireless Radar Sensor Mote for Target Material Classification."

Khan M. Iftekharuddin, Ph.D.
Major Professor

We have read this thesis and recommend its acceptance:

Robert Kozma, Ph.D.

Aaron L. Robinson, Ph. D.

Accepted for the Graduate Council:

Karen D. Weddle-West, Ph.D.
Vice Provost for Graduate Programs

AUTONOMOUS WIRELESS RADAR SENSOR MOTE FOR TARGET MATERIAL CLASSIFICATION

by

Muhammad Mahmudur Rahman Khan

A Thesis

Submitted in Partial Fulfillment of the

Requirements for the degree of

Master of Science

The University of Memphis

December, 2010

Acknowledgements

First of all, I express my sincere gratitude to almighty GOD for HIS immense blessings to my life and in this work. I would like to thank my academic advisor Dr. Khan M. Iftekharuddin for his valuable and continuous guidance and encouragement .I also like to express my gratitude to the members of my thesis committee, Dr. Robert Kozma and Dr. Aaron L. Robinson for their precious directions and support.

I am also grateful to all the members of ISIP lab for their kind support and continuous encouragement. I also extend my sincere gratitude to Ms. Becky Ward for her comprehensive support during my academic period here in University of Memphis. I also like to express my sincere thanks to Mr Thomas E. Wyatt for allowing me to use the equipments from his electrical circuit lab for doing experiments.

Finally I like to extend my gratitude to FedEx Institute of Technology at University of Memphis for funding this work partially through a project of Center for Large-Scale Optimization and Networks (CLION).

ABSTRACT

Khan, Muhammad Mahmudur Rahman.M.S.The University of Memphis. December, 2010. Autonomous Wireless Radar sensor Mote for Target Material classification. Major Professor: Khan M. Iftekharuddin, Ph.D.

An autonomous wireless sensor network consisting of different types of sensor modalities is a topic of intense research due to its versatility and portability. These types of autonomous sensor networks commonly include passive sensor nodes such as infrared, acoustic, seismic, and magnetic. However, fusion of another active sensor such as Doppler radar in the integrated sensor network may offer powerful capabilities for many different sensing and classification tasks. In this work, we demonstrate the design and implementation of an autonomous wireless sensor network integrating a Doppler sensor into wireless sensor node with commercial off the shelf components. We also investigate the effect of different types of target materials on return radar signal as one of the applications of the newly designed radar-mote network. Usually type of materials can affect the amount of energy reflected back to the source of an electromagnetic wave. We obtain mathematical and simulation models for the reflectivity of different homogeneous non-conducting materials and study the effect of such reflectivity on different types of targets. We validate our simulation results on effect of reflectivity on different types of targets using real toy experiment data collected through our autonomous radar-mote sensor network.

Table of Contents

LIST OF FIGURES

LIST OF TABLES

Chapter 1

Introduction

An autonomous wireless sensor network with different sensor modalities is an active research focus due to its versatility and portability of applications [1]-[5]. An autonomous sensor network is a collection of sensor nodes with limited processing, power, and communication capabilities that monitors a real world environment without no or limited human intervention. Each node of the network gathers information about the local environment, preprocesses the data, and transmit via wireless channels to a base station [1]. Historically, this type of autonomous system has used infrared, acoustic, seismic, and magnetic sensors for passive sensing, and optic and ultrasound sensors for active sensing. However, RAdio Detection And Ranging (Radar) has been conspicuously absent in sensor networks [2]. Radar systems are widely used in defense, meteorology and surveillance due to their versatility in working from a long range, in adverse weather where other sensors may be unavailable, or with non cooperative targets. Radar is an object detection system that uses electromagnetic waves to identify the range, altitude, direction, or speed of moving and fixed objects such as aircraft, ships, motor vehicles, clouds, storms and terrain [6]. In addition to the precise measurements about the target objects, radar systems have the capability to classify targets into different classes based on the Radar Cross Section (RCS) of different classes of objects. The capability of such classification is related to the electromagnetic energy reflected back from different classes of objects. The types of materials affect the amount of reflection from an object.

Electromagnetic waves through matter are governed by the permittivity, the permeability, and the conductivity of the materials [7][8]. The widespread commercial applications of the radar have been limited because the conventional systems are expensive, bulky, and difficult to use with very few exceptions [2]. Currently, with the advancement of technology many small inexpensive radar sensors with standard capability and low power requirements are commercially available [9]. Therefore, there is an opportunity to integrate a radar sensor with autonomous distributed wireless sensors.

The integrated autonomous sensor system including radar sensors will add a powerful and robust sensing modality to the already available modalities such as acoustic, magnetic, vibration, and passive infrared sensors in wireless sensor node. Effective and intelligent design of such integration can provide a powerful distributed sensor network system with versatile and complementary sensor modalities. In the integrated system, radar offers measurements of the range, velocity, direction, and electromagnetic characteristics of the target to complement existing wireless sensor node capabilities. The intelligent combination of some or all of the sensor modalities in certain application scenarios can work as an effective tool to detect, track, and identify targets in wide areas. The intelligent and successful design and implementation of such an integrated autonomous distributed sensor network, may work as a low tier data gathering system for an intelligent decision support system. Furthermore, the successful development of this type of system using the commercially available low-cost products would be more useful for widespread civil and military

applications. There have been some efforts to integrate a Doppler sensor to the wireless sensor node in recent years. We discuss them briefly in Chapter 2. BumbleBee is a wireless node with radar integrated [11]. The Radar in BumbleBee operates in C-Band (5-8GHz). BumbleBee claims to detect velocity of moving objects with built in micro strip antenna. We plan to integrate a K_a – band (24-40GHz) Doppler Radar into the wireless node which will detect range and velocity of target object simultaneously. We also use horn antenna which sends signal more specific to a target direction. Moreover, our target is to build the system with cheap, commercially available off the shelf components.

In this thesis, we design and implement an autonomous distributed sensor network that integrates a low-cost tiny Doppler radar sensor with the commercially available wireless sensor motes for dynamic surveillance and tracking. Our autonomous distributed sensor network is then used to collect data from an indoor experimental setup. The data collected from the network is stored and analyzed in a computer system connected to a base station. The first part of the thesis deals with design and implementation of autonomous sensor network by integrating a Doppler radar sensor to the commercially available wireless sensor mote. Then we exploit the integrated wireless mote to collect Doppler to compute the range and velocity of moving targets. The second part of the thesis investigates the effect of different types of materials on the amount of reflectivity for Doppler radar using the same integrated sensor. The material property is an important factor that influences how much electromagnetic energy is reflected back to the source from where it emits. For simplification of the model and limited

scope of this thesis, we just investigate the reflectivity of the non- conducting materials .Since the non-conducting materials have constant permittivity and no conductivity, the index of the refraction is constant and real valued for different types of materials of this class[7][8]. Therefore, increasing the index of refraction increases the reflections emitting back from the material.

We investigate the reflectivity property of different non-conducting target materials to classify objects. The refractive index of non-conducting materials and the reflectivity of plain electromagnetic wave from non-conducting materials can be modeled mathematically [7][8]. We modify the reflectivity model to incorporate Doppler principle and simulate the effects of Doppler signal reflected from non-conducting materials. Then reflectivity indices for the same non-conducting materials are validated by experimentally collecting radar reflection data from non-conducing material surfaces using our integrated radar-mote autonomous system. The simulated radar signal is compared with that of experimental signal for verification. Finally, we classify different types of non-conducting materials based on the radar signals reflected back from the corresponding material surfaces using Multiple Signal Classification (MUSIC) signal processing technique.

In summary, the objectives of this thesis can stated briefly as following list,

1. To design and implement a wireless autonomous radar mote sensor network integrating a Doppler radar into wireless sensor node with low cost commercial off the shelf components.

2. To investigate the effect of different types of target materials on return radar signal and use the newly built integrated radar mote sensor network as data collection tool for the investigation.

In Chapter 2, we review relevant background research and the essential technologies required for this thesis. In Chapter 3, we discuss the proposed design and implementation of an integrated radar-mote autonomous system. Chapter 3 also discusses the modified reflectivity model to show how material property affects the reflection of electromagnetic waves. We discuss the theoretical derivation of the modified velocity model used to simulate the reflection of electromagnetic waves from a few non conducting materials. We also discuss a simple signal processing algorithm to classify different types of materials in Chapter 3. In Chapter 4, we show experimental implementation of our radar-mote design and discuss data collection using our integrated experimental setup. The comparison between simulated and experimental reflectivity of non-conducting materials are also shown in Chapter 4.The successful classification of different types of non-conducting materials based on the electromagnetic reflection from surface of different materials is further demonstrated. Finally, we discuss our conclusion and future work in Chapter 5.

Chapter 2

Background Review

In this Chapter, we discuss relevant background related to the constituent parts of our autonomous wireless network such as Doppler radar sensor and wireless sensor motes. The capability of the sensors is also discussed from theoretical point of view. The theoretical model showing the relation between material refractive index and reflectivity of electromagnetic signal is discussed as well [7][8]. In this Chapter, relevant recent research efforts about integrating radar sensor with wireless motes and their intended applications are also reviewed.

One of the goals of our thesis is to design and implement an autonomous sensor network integrating a Doppler radar to a wireless sensor mote with the commercial off the shelf (COTS) components effectively to provide the complementary benefits of different sensor modalities. The need for such an integrated sensor network suite is discussed in the Chapter 1.

2.1 Previous Research efforts on integrated radar-mote sensor networks and their Applications

The sensor network research field is a relatively new field. Miniature autonomous sensor networks that include different types of sensor modalities such vibration, acoustics, temperature, and pressure are developed as a result of industry-academia cooperation. Historically, surveillance systems have used infrared, acoustic, seismic and magnetic for passive sensing, and optics and ultrasonic for active sensing. However, radar has conspicuously absent [2]. Because radar

systems are conventionally bulky and requires, such systems are not suitable for autonomous wireless sensor network platform. With the advent of the micro-power pulse radar at Lawrence Livermore National Labs [30] in mid 1990s, the low power radar becomes a possibility. Subsequently, technical progress in sensor network led the effort to integrate radar as one of the sensor modalities to sensor network platform. There have been a few successful efforts to integrate radar in sensor mote designed by a group of researcher from UC Berkeley and Ohio State University [2].

The Radar mote, designed by researchers at UC Berkeley and Ohio State University, consists of several circuit boards including a main processor and radio board, an optional sensor board, an ultra wideband radar sensor, and a power board [2]. Reference 2 uses Mica2 sensor mote and 2.4 GHz TWR-ISM-002 radar sensor from Advantaca [10] as two main components of their radar-enabled sensor network. The integration also includes a custom designed power board which provides power required for the radar and other equipments, and an optional Mica sensor board. These circuit boards are housed in a self-righting enclosure that ensures the radar's antenna is always oriented vertically [2]. The authors in Ref 2 use a network of twelve Radar Motes in a surveillance application to successfully detect, classify, and track people and vehicles in an experimental scenario with moving targets [2].

BumbleBee is another integrated radar mote sensor developed by the Samraksh Company [11]. The Radar used in BumbleBee is a low-power Pulsed Doppler Radar (PDR) that is designed to suit a variety of Wireless Sensor Network (WSN)

applications. Unlike traditional radars, the BumbleBee is designed to be compatible at a systems level with small, battery powered nodes [11]. The BumbleBee operates at a 5.8GHz center frequency. The key features of the BumbleBee include: a detection range between 1m to 10m which is controllable via software, coherent output (both I and Q channels), on-board internal antenna, 60 degree conical coverage pattern, and detection of radial velocities between 2.6cm/sec and 2.6m/sec [11]. The BumbleBee package includes a BumbleBee radar board, a cable to connect the BumbleBee radar board to the TelosB mote or TMote Sky, three alkaline batteries in a battery case, a clear plastic base, four 2 inches post for separating the board from base and supporting software [11]. The supporting software of the BumbleBee includes three modules such as: a device driver providing the interface between BumbleBee radar board and TelosB mote, a data acquisition program, and a simple detector program [11]. The programs are written in TinyOS 2.x platform. The BumbleBee is suitable for variety of monitor and surveillance applications including classification of human activities in commercial and recreational settings, and monitoring industrial machinery during operation, and monitoring livestock or wildlife activity [11].

Although these integrated radar-mote sensor network products work well for certain applications, there is still room for improvement. The radars used in the above mentioned platform offer the velocity of a moving target. Per manufacturer's claim the BumbleBee claims to have the capability to compute range also after complex signal processing. However, it is not produced simultaneously with velocity. Our plan is to improve this drawback of the system

mainly along with other improvements. Our radar-mote system will compute the range and velocity simultaneously with simple signal processing technique. We also plan to sample the signal with higher rate which will give more points for each signal and the signal is smoother.

2.2 Autonomous sensor network

An autonomous sensor network is a collection of sensor nodes with limited processing, power, and communication capabilities that monitors a real world environment through differing modalities. The nodes gather information about the local environment, preprocess the data, and transmit via wireless channels to a base station [1]. Generally a wireless sensor network consists of spatially distributed wireless sensors to cooperatively monitor physical or environmental conditions such as temperature, sound, vibration, pressure, motion and pollutants [3][5]. The development of wireless sensor networks was at first motivated by military applications such as battlefield surveillance. However, they are now used in many industrial and civilian application areas, including industrial process monitoring and control, machine health monitoring, environment and habitat monitoring, healthcare applications, home automation, and traffic control [3][4][12]. Figure 1 shows the typical organization of an autonomous wireless sensor network.

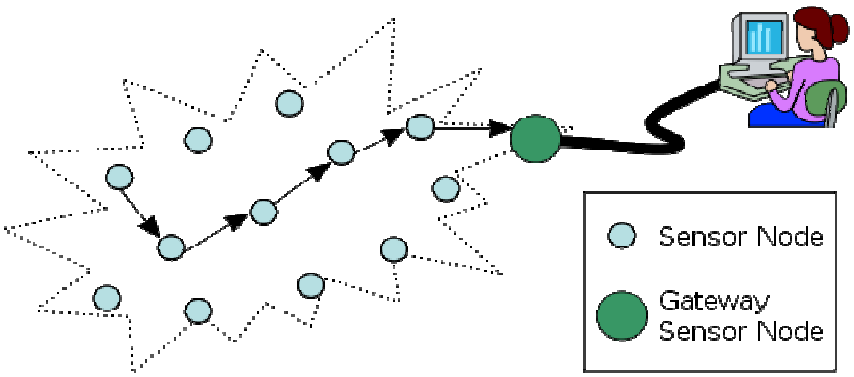

Fig. 1: Typical Wireless Sensor Network Architecture.

In addition to the one or many sensors incorporated in the sensor node each node is typically equipped with a radio transceiver or other wireless communication device, a small microcontroller and an energy source, usually a battery [3].

2.2.1 Applications of autonomous sensor network

Although a large percentage of sensor network research is initiated by military research organizations, sensor networks have found application in a broad spectrum of non-military applications.

In cases of habitat monitoring, the sensors are deployed in remotes area to monitor the activities of habitats of that area. Wild life scientists can effectively use the sensor network for monitoring different wild life activities without human intervention [13]. Wireless sensor networks have been used successfully to monitor different environmental conditions. The sensors are deployed in large geographic areas to collect data sensing different physical conditions such as

temperature, heat, pressure, level of water [14]. Health applications of wireless sensor network span from physiological data collection for humans to tracking and monitoring the doctors and patients in hospitals. Smart Sensors and Integrated Microsystems (SSIM) is a promising project by a group of scientist where a retina prosthesis chip consisting of 100 micro sensors are built and implanted in human eye [15]. A few other similar applications include glucose level monitors, organ monitors, cancer detectors and general health monitors [16]. In the battlefield, a large number of wireless sensor nodes with different kinds of sensor modalities are deployed to detect intrusion and track the intruder. The surveillance system in civil application also uses wireless sensor networks very effectively to monitor any area.

2.2.2 Sensor Node Architecture

A typical wireless sensor node has four basic components including a sensing unit, a processing unit or microcontroller, a transceiver unit, and a power unit [17]. Figure 2 shows typical sensor node architecture. Senor unit or sensing unit is the most important component of wireless sensor network.

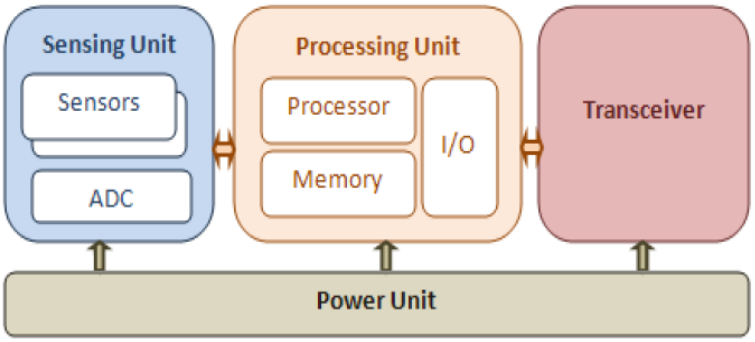

Fig. 2: Major components of a typical wireless sensor node (Ref. [12])

In addition to these major components a sensor node can include a global positioning system or some other specific component based on the applications. Most of the commercial sensor nodes provide expansion slots to support the addition of application specific components to the existing system node.

Sensing Unit or Sensor

A sensor or sensing unit is a device that measures some physical quantity and converts it into a signal to be processed by the microcontroller [17]. The sensing unit generally senses the measurable change of any physical condition continually within a certain range of its operation. The general sensing modalities available with the commonly available sensor units are temperature, vibration, acoustic, magnetic field, pressure sensors. The sensing units may be classified as an active or passive based on the sensing methods. Passive sensors gather data from environment without actual probing or manipulation of the environment. Passive infrared sensing is such a sensing modality. However, for active sensing the sensors collect data with active manipulation of the environment. Radar, sonar and some seismic sensors fall into the category of the active sensors. The active sensors, such as radar, generate probing signals, send them to the environment and receive the reflected signals. According to the direction of sensing, the sensor can be further classified into directional and omni-direction classes. Generally, most of the passive sensors such as vibration, acoustic, magnetic sensors are omni-directional since these sensors sense the measurable physical change in all directions around the sensors. Directional

sensors such as radar and sonar send directed signal beams through some directional antenna and receive the reflected response through antenna.

Microcontroller

A microcontroller, the processing unit in a wireless sensor node, processes the sensed data, controls and coordinates different activities and parts of the sensor nodes efficiently. Microcontrollers are preferred because of their low power consumption, flexibility, and expandability which are very important issues for a sensor node.

Transceiver

A transceiver is a device with which a sensor node forms a network with other sensor nodes by transmitting and receiving signals from other nodes. Both the network control signals and the sensed data are transmitted through different channels by the transceiver units of the sensor nodes. The sensor node transceiver unit generally uses the Radio Frequency (RF) for communication .The Industrial, Scientific and Medical (ISM) radio frequency band is commonly used as the standard radio frequency band of communication for sensor transceivers.

Power Source

The power source in case of sensor node is generally storage energy cells or battery. Although some sensors include solar cells as power sources they may

not be suitable for all application scenarios. Some sensors can even renew their energy from sensed vibration and temperature.

Memory

Sensor nodes need to have some kind of memory to store programs and data. The obvious choice of memory for sensor node is built in on chip memory from energy and efficiency perspective. But the standard sensor nodes also provide some external memory for extended user application in mind.

2.2.3 Commercial Wireless Sensor Mote Products

The wireless sensor network field is still a developing field and several standards are either being ratified or under development. We summarize the features of some of the commercially available standard wireless node products in Table 1.

Table 1: List of commercially available sensor nodes [18][19]

Sensor Node Name and Picture	Micro-controller	Transceiver	Program and data Memory	External memory	Programming	Operating System Support
IMote 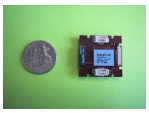	ARM core 12 MHz	Bluetooth with the range of 30 m	64K SRAM	512K Flash	nesC	TinyOS support
Mica2 	ATMEGA 128L	Chipcon 868/916 MHz Chip	4K RAM	128K Flash	nesC	TinyOS, SOS and MantisOS support
MicaZ 	ATMEGA 128L	TICC2420 802.15.4 or ZigBee compliant radio	4K RAM	128K Flash	nesC	TinyOS, SOS, MantisOS, Nano-RK support

TelosB 	Texas Instruments MSP430 Micro-Controller	250 kbit/s 2.4GHz IEEE802.15.4 Chipcon Wireless Transceiver	10K RAM	48K Flash	nesC	TinyOS, SOS, MantisOS, Contiki Support
T-Mote sky 	Texas Instruments MSP430 Micro-Controller	250 kbit/s 2.4GHz IEEE802.15.4 Chipcon Wireless Transceiver	10K RAM	48K Flash	nesC	TinyOS, SOS, MantisOS, Contiki Support
Iris Mote 	AT mega 128	Atmel AT86RF230 802.15.4/ZigBee compliant radio	8K RAM	128K Flash	nesC	TinyOS, MoteWork support
BTnode 	Atmel ATmega 128L (8 MHz @ 8 MIPS)	Chipcon CC1000 (433-915 MHz) and Bluetooth (2.4 GHz)	64 + 180 K RAM	128K Flash and 4K EEP-ROM	C and nesC	BTnut and TinyOS Support
Dot 	ATMEGA 163L		1K RAM	8-16K Flash	weC	

We have selected TelosB mote for the design and implementation of our integrated radar-mote system. Because, TelosB platform is widely accepted and used by people who work with sensor network. It also supports different light-weight operating system including TinyOS. Therefore, it is reasonable to start with the TelosB platform although we plan to make the system generic for all platforms in the future.

2.2.4 TelosB Mote Platform Details

Crossbow's TelosB mote (TPR2400) is an open source platform designed cutting-edge implementation for the research community [23]. The TPR2400 includes the standard features such as USB programming capability, an IEEE 802.15.4 standard radio transceiver with built in antenna, a low power microcontroller (MSP430), and capability to integrate sensor boards through standard ports. The TelosB is successfully used in applications such as low power sensor network development and sensor network experimentation by many research groups all over the world. TelosB runs TinyOS 1.1.10.Tiny OS is a small, energy efficient operating system designed specifically for sensor nodes. The key features of the TelosB mote platform are as follows [20],

a) IEEE 802.15.4/ZigBee compliant RF (Radio Frequency) transceiver
b) Uses a globally compatible ISM band (2.4 to 2.4835GHz) for wireless communication between nodes with 20kbps data rate.
c) Integrated on board antenna with 20m to 30m range in indoors and 75m to 100m range in outdoors.
d) 8MHz Texas instruments MSP430 microcontroller with 10kB RAM.
e) 1MB external flash for data logging
f) Programming and data collection using USB interface
g) Low current consumption
h) Optional sensor suite including integrated light, temperature and humidity sensor

Figure 3 shows the block diagram and a real picture of TelosB mote.

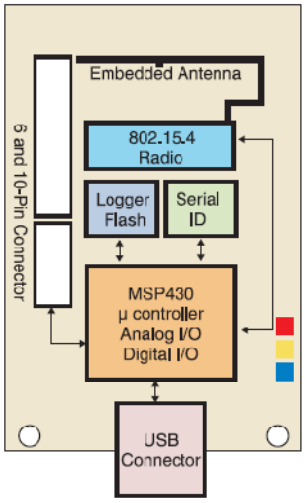

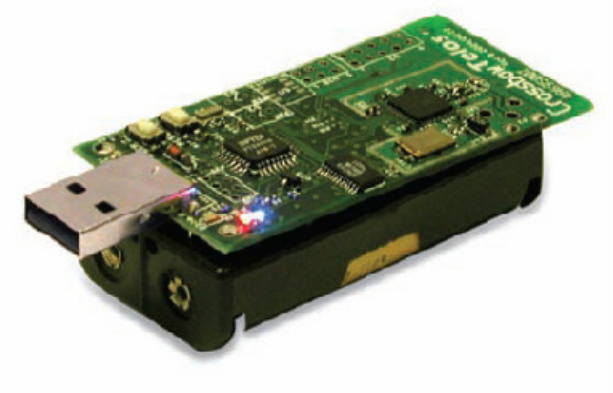

Fig. 3: a) Block diagram of TelosB TPR2400 mote (left), b) TelosB TPR2400 mote real picture (right).(Ref.20)

Microcontroller in TelosB (TI MSP430)

The central processing unit in a TelosB mote is Texas Instruments MSP430 microcontroller. The key features of the MSP430 microcontroller are as follows [21],

a) Ultra low power architecture which extends battery life.
b) High performance analog and digital I/O system for precise measument.The MSP430 has 8 external ADC ports and 8 internal ADC ports. We can use the internal ADC ports to read internal thermistor or monitor the batter voltage. The external ADC ports which are available as part of expansion connectors to add optional sensor board or any analog

sensor can be used to read analog signal from the sensor. We will use one of the analog ports to read our radar output signal.

c) The 16bit RISC processor controls the TelosB activities very efficiently and allows designing new application by programming.
d) In-system programmable flash permits the flexible code changes, field upgrades and data logging.
e) High speed UART (Universal Asynchronous Receiver /Transmitter) serial communication with the laptop.

Analog to Digital Converter Module in TI MSP430

MSP430 has a high speed analog to digital converter ADC12. It supports fast 12 bit analog to digital conversion. The key features of the ADC12 module are as follows [21],

a) It can sample as fast as 200ksps.
b) Monotonic 12 bit converter with no missing code.
c) Conversion can be initiated by software or Timer_A and Timer_B.
d) Software selectable on chip reference voltage generation (1.5V or 2.5V).
e) Software selectable internal or external reference voltage.
f) Selectable conversion clock source.
g) Single channel, repeat-single- channel, sequence and repeat-sequence modes of conversion.

The ADC12 module can be configured with user software. We develop our own code module for configuring the ADC for the required operations specific to our

goal. We discuss the software level integration design in later sections. The ADC core converts an analog input to its 12 bit digital representation and stores the result in conversion memory. We can use two reference voltage levels V_{R+} and V_{R-} which are selectable by programming. Here V_{R+} is the upper limit and V_{R-} is the lower limit of converted voltage output. The digital output N_{ADC} is equal to the maximum or full scale value when input signal is equal to or more than V_{R+} .Similarly the digital output is zero when the input signal is equal to or less than V_{R-} .The formula of converting analog signals to digital is represented in following equation (1),

$$N_{ADC} = 4096 * \frac{V_{in} - V_{R-}}{V_{R+} - V_{R-}} \quad . \qquad (1)$$

We can turn off the ADC12 when not in use to save power. The MSP430 microcontroller has an on chip clock, ADC12CLK, which is used both as a conversion clock and to generate the sampling period when the pulse sampling mode is selected. There are eight external and four internal analog signal inputs in MSP430 which can be selected as the input channels for conversion by the analog input multiplexer. The channel which is not selected to take input is generally isolated from the ADC. An intermediate node is then connected to the analog ground (AV_{ss}) which helps to eliminate cross talk by grounding stray capacitance.

The ADC12 module contains a built-in voltage reference with two selectable levels such as 1.5V and 2.5V [21]. We can choose the either of the reference

voltages internally by programming. The external reference voltage can be given on pin V_{REF+} .When we want to use the internal reference we need to enable it by setting the REFON.There is another flag REF2_5V which can be used to choose between the reference voltages. If we set the lag REF2_5V=1 then the internal reference voltage is set to 2.5 whereas if we set it to 0 the reference voltage 1.5 is selected. We can even turn off the reference voltage when it is not in used to save power by programming. The modes of operations are as follows [21],

a) Single channel single conversion(A single channel is converted once)
b) Sequence of channels(A sequence of channel is converted once)
c) Repeat single channels(A single channel is converted repeatedly)
d) Repeat-sequence-of channels(A sequence of channels is converted repeatedly)

In our integration we use the second mode of operation where a single input channel is converted repeatedly until a signal to pause comes from base station. The ADC12 module can be configured with the user software. We have our code modules for configuring the ADC for the required operations specific to our goal. We will discuss about the software level integration design in later sections.

Radio Transceiver (CC2420) and Antenna in TelosB

TelosB mote uses the Chipcon CC2420 RF transceiver for wireless communication purpose. The CC2420 is true a single-chip 2.4GHz IEEE 802.15.4 compliant RF transceiver designed for low power and low voltage wireless applications. There is extensive hardware support to facilitate features

such as packet handling, data buffering, burst transmissions, data encryption, data authentication, clear channel assessment, link quality indication, and packet timing information. TelosB has an integrated on board antenna enabled but if any application requires an external or specific antenna an external Subminiature version A (SMA) connector available in TelosB to add an external antenna. The internal antenna is an Inverted-F microstrip antenna with unidirectional radiation patterns. The approximate range of the onboard antenna is 20m to 30m in indoors and 75m to 100m in outdoors which are enough for many applications.

TelosB Expansion Connector

TelosB has two sets of expansion connectors which may be configured to allow the additional devices to be connected with the mote. The additional devices can be any analog sensor, light display or digital peripherals conforming to the standard of the TelosB mote. The two expansion connectors are: 10-pin IDC header at position U2 and a 6-pin IDC header at U28 [22]. The 10-pin connector has both the analog and digital inputs. Peripherals can be connected to the 10-pin connector using an IDC header, IDC ribbon cable, or by a custom designed printed circuit board that solders directly onto the IDC header providing a robust connection to the module [22]. In our experimental integration we have used normal circuit wires to connect Doppler radar, with the expansion connector of the wireless mote. There is an additional 6-pin connector which is located in U28 position of the TelosB. The 6-pin connector provides two more analog input channels which are also used as 12bit DAC output. The following figures show

the organization of different pins in the expansion connectors. Figure 4 shows 10-pin expansion connector.

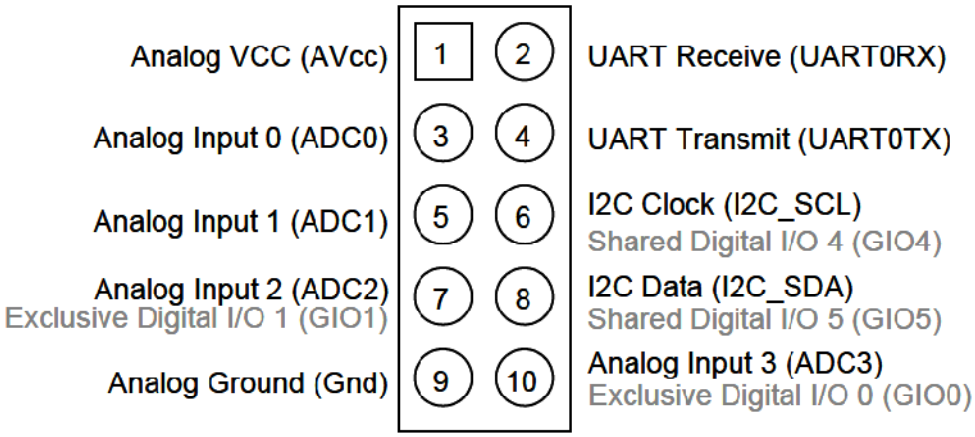

Fig. 4: The organization and functionality of the 10-pin expansion connector. The gray texts provide the alternative functions of the pins. (Ref. [24])

2.2.5 TinyOS and Programming TelosB

As the sensor nodes have limited memory and energy sources, the operating system should be very memory and energy efficient without losing the robust programming capability required for different applications. There are some embedded operating systems for wireless network platforms such as TinyOS, SOS, and Mantis-OS, Moteworks, and peerOS. Among them TinyOS, a component based operating system built specifically for the wireless sensor network platform, is widely accepted and supported by both the sensor network research community and commercial manufacturers [22][23].

TinyOS is an embedded operating system written in the Network Embedded System C (nesC) programming languages as a set of cooperating task and processes [23]. nesC is a special dialect of the C programming language that is optimized to facilitate the efficient use of very limited memory of sensor network components. The application programs on TinyOS sensor platforms also written in nesC. The supplementary tools needed to run applications are in Java and some shell scripts. The associated libraries required, such as nesC compiler and binding utilities like toolchains are mostly written in C programming language [23]. TelosB sensor platform supports TinyOS and nesC.

The TelosB motes are programmed through the onchip USB connector available in motes. TelosB uses a USB controller chip from Future Technology Devices International (FTDI) to communicate with the host computer [22]. The driver for FTDI must be installed in host computer to communicate with the TelosB mote. If the driver is installed the TelosB mote appears as COM port in windows and a device in Linux or UNIX device list. TinyOS supports programming TelosB mote.

2.3 Doppler Radar

Doppler radar system is special type of radar that exploits Doppler effect to measure the range and velocity of a target object [24]. The Doppler effect or Doppler shift is the change in frequency of a wave for an observer moving relative to the source of the wave [25]. The waves generally propagate in a medium and the velocity of the observer and the source are relative to the medium in which the wave propagates. The total Doppler Effect may therefore

result not only from the motion of the sensor and observer but also from the motion of the medium. However, if the wave, such as light, does not require a medium only the relative difference between velocity of the source and observer is considered [24]. If the source of the signal wave is fixed or static, the relative difference between the source and observer is the function of the velocity of the moving observer. Using this principle the Doppler radar emits microwave signal towards the target and the reflected signal from moving target is received and compared with the emitted signal to find the relative shift or Doppler shift which is function of target velocity. The mathematical principle to find the velocity and range using Doppler radar will be discussed in a later section.

2.3.1 The Components of a Doppler Radar

The Doppler radar consists of four major components such as transmitter, receiver, antenna, and transmit-receive switch. Figure 5 shows the block diagram of typical radar system.

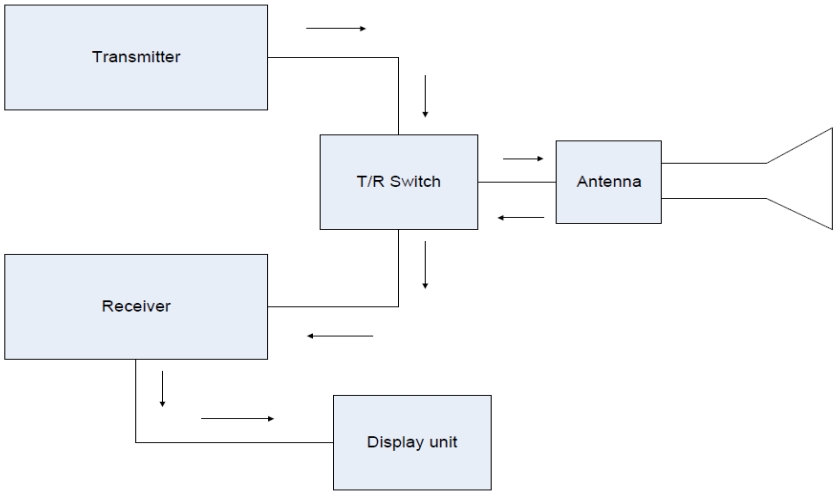

Fig. 5: A typical radar system

The transmitter generally includes an oscillator which generates signal wave of required frequency and emits toward the target or environment. Based on the target application domain the signal wave is directed to the environment in different ways using different types of antenna. An omni-directional antenna directs the signal in all possible directions. The directional antenna directs the signal wave towards a target. The receiver detects the reflected signal from a target through antenna, amplifies it as the reflected signal is weak compared to transmitted signal due to scattering loss, and sends it to a mixer. The mixer compares it with the transmitted signal to find out the frequency shift or Doppler shift which eventually helps to compute the velocity and range of a target. The transmitter and receiver unit may be in separate setup and use separate antennas, or they may be built in together sharing same antenna working as one electronic package. In case where they are bundled together with shared antenna and some other components, there should be an electronic switch to control the mode of transmitting and receiving. When the transmitter and receiver are bundled together it is termed as transceiver. We will use such a Doppler transceiver for designing our experimental system.

2.3.2 Different Frequency Band Radars and their Applications

For the electronic and electrical devices the Institute of Electrical & Electronic Engineers (IEEE) standard is followed by almost all manufacturers. In addition to this device standard, different countries may have their own standard of allocating frequency band for different applications. Table 2 shows a brief list of

the radar frequency band which are widely adopted in USA by IEEE and internationally by International Telecommunication Union (ITU).

Table 2: Radar Frequency Band [26]

Frequency Band Name	Frequency Range	Wavelength Range	Application
HF(High Frequency)	3-30MHz	10-100m	This radar is used to detect target at very long range like thousands of kilometers. The coastal radar systems generally use this band of radars.
P	< 300MHz	> 1m	Here 'P' stands for previous which is applied retrospectively to earlier radars systems.
VHF(Very High Frequency)	30-330 MHz	0.9-6M	Used in radio broadcasting (FM radio, amateur radio), television broadcasting, mobile earth station, radio modems, and air traffic control.
UHF(Ultra High Frequency)	300-1000 MHz	0.3-1m	This range is widely used in GSM mobile cellular communication now. Also used in ground penetrating radar, television signal transmission, RFID (Radio Frequency Identification) tag
L	1-2 GHz	15-30 cm	The name 'L' comes from long. This band was earlier used only for military application like long range air traffic control and surveillance. This band is now used for mobile communication (GSM 1800 and 1900).GPS carriers also use this band.
S	2-4GHz	7.5-15cm	'S' comes from short. Marine radars, long range weather radars and terminal air traffic control use this band.
C	4-8 GHz	3.75-7.5cm	Some weather radars use this band. Also used in Wi-Fi communication and cordless telephone
X	8-12 GHz	2.5-3.75cm	Used in marine radar, weather forecasting, medium resolution mapping, and ground surveillance. In USA a narrow range 10.525+/- 25MHz is used for airport radar.
K_u	12-18GHz	1.67-2.5cm	Primarily used for satellite communication.
K	18-24	1.11-1.67cm	Radar using this band is commonly used by police to detect speed of vehicles. Also used by the meteorologist for detecting clouds.
K_a	24-40GHz	0.75-1.11 cm	Used for detecting speed by police. Also used in the photo radar which is used to trigger cameras to take picture of license plates of cars by police when required. Operating range of photo radar is 34.3+/- 0.1GHz.
Mm	40-300 GHz	7.5mm-1mm	This band is still not commercially used. Used in research or experimental military radar.
UWB (Ultra Wide Band)	1.6-10.5 GHz	18.75-2.8cm	Used for Through wall radar and imaging system.

2.3.3 Radar Output

The radar output generally is of two forms such as reflectivity and velocity. Reflectivity measures the amount of precipitation exits in a particular area and velocity measures the speed and direction of the precipitation toward or away from the radar.

Reflectivity

There are different factors that influence how much electromagnetic energy will be reflected back to the source from where it emits. The factors are as follows [27],

a) The material of the target ;
b) The size of the target compared to the radar antenna ;
c) The incident angle or the angle at which the electromagnetic beam hits a particular portion of the target. This depends on the shape of the target and its orientation to the Radar source;
d) Reflected angle or the angle at which the radar signal is reflected back after hitting the target. It depends on the incident angle;
e) The strength of the signal emitted from the radar; and
f) The distance between the radar and the target.

Therefore, if all of the other factors which influence the radar reflectivity remain constant for different types of materials, we can exploit the reflectivity to classify different types of materials. For example, metals naturally tend to be good reflective materials whereas nonmetallic objects work as weak reflectors for the

microwave signals. We exploit this observation to detect and classify different target material types using our novel integrated radar-mote system.

Velocity

Most of the radars determine target velocity using the Doppler effect .The Doppler effect or Doppler shift is defined as the change in frequency of a wave for an observer moving relative to the source of the wave. When a source moves away from an observer and emits electromagnetic wave toward the observer through a medium with an actual frequency f_0 then the stationary observer relative to the medium detects the waves with frequency f given by following equation [25],

$$f = \left(\frac{v}{v+v_s}\right) f_0 \ , \qquad (2)$$

where f is the observed frequency, f_0 is the actual frequency, v is the velocity of the wave in the medium, and v_s is the velocity of the source relative to the medium. If the source moves away from the observer v_s is positive whereas if the source moves toward the radar v_s is negative.

For moving objects, one can use the same Doppler shift principle for velocity computation. Suppose a doppler radar directs a beam of waves toward a moving target. If the target is moving away from the radar each successive radar waves need to travel more distance to reach the moving target and when the waves are reflected back and detected by the radar they have some associated delay. One

can obtain velocity of the target as the speed of the wave is known. When the target moves toward the radar we can detect the range and velocity using same principle as we have all the parameters known other than source velocity in Eq. (2). The detail mathematical background of how to detect the range and velocity of a moving target using Doppler radar is discussed in section 2.4.

2.3.4 K-band Doppler Transceiver (MACS-007802-0M1R1V) Details

We select a K_a-band Doppler transceiver from M/A-Com Tech for our integrated radar-mote sensor suite. It is low- cost ($20) and low-power Doppler transceiver which suits our goal to build a low- cost, low-power integrated radar-mote sensor suite with Commercial-Off-The-Shelf (COTS). This M/A-COM RF transceiver (Model MACS-007802-0M1RSV) is primarily used for automotive applications such as front and rear-ends collision detection, in ground speed measurement, and as motion detectors in automatic door systems [28]. The transceiver is also very small in size, (<1inch on each side) resembling to an ice cube, which makes it an excellent choice for our autonomous integrated radar-mote sensor network system. The radar utilizes a Gunn diode oscillator and transmits continuous wave at 24.125GHz. The transceiver has electronic tuning system which allows varying the frequency within a bandwidth of 0.3GHz. An external voltage ramp pulse can be applied to the electronic or voltage tune input of the radar which causes the radar to emit continuous frequency modulated signal of 300MHz bandwidth. The signal received by the radar through antenna is mixed with the transmitted wave and low pass filtered to produce In-phase (I) and Quadrature (Q) output which are available on pin 3 and 4 of the radar respectively. The key features of the

Doppler transceiver include low cost, small size, low power consumption (8mW output power), motion trajectory detection,300MHz of electronic tuning,10Hz-5000Hz IF bandwidth, and lead free (Restriction on Hazardous Substances) [28]. Figure 6 and Table 3 shows the Doppler transceiver and the organization of its pins.

Fig. 6: Doppler Transceiver (MACS-007802-0M1RSV) (Source: www.macomtech.com/datasheets/MACS-007802-0M1R1V.pdf)

Table 3: Pin Configuration of the Doppler Transceiver (MACS-007802-0M1RSV) (Source: www.macomtech.com/datasheets/MACS-007802-0M1R1V.pdf)

PIN	Function
1	DC Input
2	GND
3	IF Output (Mixer 1)
4	IF Output (Mixer 2)
5	Vtune input

2.4 Radar Signal processing for finding the range and range-rate of the target

Consider that the Doppler radar transceiver emits a continuous frequency sinusoidal signal as follows [29]-[30],

$$x_0(t) = \cos(2\Pi f_0 t + \Phi), \quad (3)$$

here, f_0 is the carrier frequency, t is time and Φ is some random phase. The transmitted signal is then propagated to a stationary target, reflected, and propagated back to the Doppler transceiver. The received signal is the replica of the transmitted signal with a propagation delay corresponding to the round trip time required for the propagation of the signal. If we assume that the transmitter and receiver are synchronized with same clock, this propagation delay can be represented as

$$\Delta t = 2r/c\ , \quad (4)$$

where r is the distance between the radar and the target object in meter and c=3 x 10^8 m/sec is the propagation velocity of the microwave signal. Now the received signal can be expressed as

$$x_r(t) = \sigma x_0\ (t - \Delta t) = \sigma x_0\ (t - 2r/c\ ) = \sigma\cos[2\Pi f_0 t + \Phi - 4\Pi f_0 r/c]\ , \quad (5)$$

where σ is a constant which corresponds to the target radar cross section (RCS), geometric attenuation of the signal and other terms related to target object and signal characteristics. In the receiver end of the Doppler transceiver circuitry the received and transmitted signals are multiplied and then filtered using low pass filter. The filtered signal output from the mixer is as follows,

$$F_{mix}(t) = x_0(t).x_r(t) = \cos(2\Pi f_0 t + \Phi).\sigma\cos[2\Pi f_0 t + \Phi - 4\Pi f_0 r/c] \ . \quad (6)$$

Simplifying this mixer output using trigonometric identity,

$$2\cos a.\cos b = \cos(a+b) + \cos(a+b) \ . \quad (7)$$

We get,

$$F_{mix}(t) = \frac{\sigma}{2}\cos[4\Pi f_0 t + 2\Phi - 4\Pi f_0 r/c] + \frac{\sigma}{2}\cos[4\Pi f_0 r/c]. \quad (8)$$

This mixer output signal is the summation of two terms having frequency $2f_0$ and a constant DC bias. If the sinusoidal signal is discarded using a low pass filter we get the following signal as the radar output where the radar output is a function of target range,

$$I = \frac{\sigma}{2}\cos[4\Pi f_0 r/c]. \quad (9)$$

Now based on the range Eq. (4), the range-rate or velocity expressions are derived. If the target object is changing the range at a constant rate $\dot{r}$ meters/sec then,

$$r(t) = r_0 + \dot{r}t, \tag{10}$$

where r_0 is range at instant zero. Putting the value of r into equation (5) and rearranging the term we get,

$$x_r(t) = \sigma\cos\left[2\Pi(f_0 + \Delta f)t - \frac{4\Pi f_0 r_0}{c} + \Phi\right], \tag{11}$$

where

$$\Delta f = -(2\dot{r}/c)\, f_0. \tag{12}$$

Δf is known as Doppler frequency shift [30]. From Eq. (9), it is evident that when an object moves away from the radar it causes the reflected signal to down shift slightly relative to the transmitted signal. The radar receiver mixes the transmitted and shifted received signal and passes it through the low pass filter. The low pass filtered signal after simplification with cosine identity can be expressed as,

$$I(t) = \frac{\sigma}{2}\cos\left[2\Pi(\Delta f)t - \frac{4\Pi f_0 r_0}{c}\right]. \tag{13}$$

This final radar output oscillates at Doppler frequency Δf.Equation (10) we see that Doppler frequency is proportional to range-rate or velocity of the target object. We can get the magnitude of range-rate $\dot{r}$ by capturing the $I(t)$ signal with a storage oscilloscope and then computing the Fast Fourier Transform (FFT).

By using the I component of the Doppler data it is possible to estimate the target velocity by sampling the outputs with an oscilloscope and applying FFT. However, if we use the I channel data only we cannot determine the direction of movement without ambiguity. By using the Quadrature component (Q) of dual channel radar we can combine I and Q into a complex signal,

$$F(t) = I(t) + iQ(t) \ , \tag{14}$$

where Q-channel data is the 90 degree phase shifted version of the I-channel data. Now applying FFT to the complex signal allows us to get rid of the twin peaks. In our experiment we capture I-channel and assign zero to the Q-channel. In the next section we briefly describe using ramp pulses for computing range and velocity based on the above discussion.

We use a Doppler radar which has an electronic tuning input with frequency band 24 to 24.3GHz. By applying different voltages to the electronic tuning input we can vary the frequency from a minimum value f_0 to a maximum value f_1 between 24 to 24 GHz. In the next section, we discuss how we can use this frequency variation to measure target range and velocity. To cover the frequency band

quickly we use ramp voltages as voltage tune input which generates a continuous sweep from low to high frequency. This type of sweep is known as chirp signal. We can express the transmitted chirp signal using following equation,

$$x_0(t) = \cos\mathrm{A}(t), \tag{15}$$

here,

$$A(t) = 2\Pi f_0 t + \frac{\Pi(f_1 - f_2)}{T} t^2 \ , \quad . \tag{16}$$

where f_0 and f_1 are minimum or starting and maximum or ending frequencies of the chirp signal respectively and T is the time duration of one ramp cycle.

The transmitted signal is propagated to the target object from radar focused using horn antenna. The transmitted signal is reflected and propagated back to the receiver. We assume that the transmitter and receiver are co-located and synchronized. So the signal received by the radar is the replica of transmitted signal with a round trip propagation delay Δt to the target object. We can express the received signal as,

$$x_r(t) = \sigma x_0\ (t - \Delta t) = \sigma\cos\mathrm{A}(t - \Delta t) = \cos\left[2\Pi f_0\ (t - \Delta t) + \frac{\Pi(f_1 - f_0)}{T}(t - \Delta t)^2\right], \tag{17}$$

where σ is RCS plus geometric attenuation etc. as we discussed earlier. We can rearrange the terms in the above equation and get the received signal expressed as,

$$x_r(t) = \sigma\cos[A(t) + \Phi(t)] \ , \tag{18}$$

where $A(t)$ is same as showed in Eq.(16) and $\Phi(t)$ can be expressed as,

$$\Phi(t) = -2\Pi\Delta t f_0 \ + \frac{\Pi(f_1 \ - f_0\,)}{T}(\Delta t)^2 - \frac{2\Pi(f_1 \ - f_0\,)}{T}(\Delta t)t \ . \tag{19}$$

we have derived the in-phase (I) output expression in Eq.(9).Equations (6)-(8) show how we can express the receive signal as summation of two terms. Using the same derivation procedure we can get the received signal as the summation of two terms in case of chirp signal pulses as,

$$F_{mix}(t) = \frac{\sigma}{2}\cos[2\mathrm{A}(t) + \Phi(t)] + \frac{\sigma}{2}\cos\Phi(t). \tag{20}$$

Putting the values of $\mathrm{A}(t)$ and $\Phi(t)$ from Eqs. (17) and (19) respectively, we get a new expression for Eq. (20).The the former term in Eq. (20) is a chirp having minimum frequency $4\Pi f_0$ and the later term is a cosine oscillation of frequency $\frac{2\Pi(f_1 \ - f_0\,)}{T}(\Delta t)t$. As the transmitted pulse is narrowband that means

$f_0 \ \gg (f_1 \ - f_0\,)$,so we can discard the first term using a low pass filter from signal represented by equation (17).The in-phase (I) signal can be expressed as,

$$I(t) = \frac{\sigma}{2}\cos \Phi(t) \ . \tag{21}$$

Now we substitute the value of $\Phi(t)$ from Eq. (19) to Eq. (21) to obtain the relation between cosine signal and range of the target object. In Eq. (21) we discard terms containing f_0 as it is large compared to the Doppler frequency and as we have used low pass filter for getting the I signal. Finally the I signal can be expressed as,

$$I(t) = \frac{\sigma}{2}\cos\left[\frac{4\Pi f_0 r_0}{c} + \frac{4\Pi(f_1 - f_0)r}{cT}\mathrm{t}\right] \ . \tag{22}$$

Similarly, we can get the Q output as,

$$Q(t) = -\frac{\sigma}{2}\sin\left[\frac{4\Pi f_0 r_0}{c} + \frac{4\Pi(f_1 - f_0)r}{cT}\mathrm{t}\right] \ . \tag{23}$$

Finally, we discuss computing range and velocity using multiple chirp pulses which in our case is ramp pulses. If we assume that the target is moving with a constant velocity and we express the motion as

$$r(\xi) = r_0 + \dot{r}\xi \ , \tag{24}$$

where $r_0$is the range of the object at time instant zero, $\dot{r}$ is range-rate or velocity of the target object and ξ is called slow time. The time at which each successive pulse is transmitted from the radar is known as slow time and fast time is the

typical time taken by the signal propagation. If we substitute the value of r from Eq. (24) into the Eqs. (22) and (23), we get the following two new equations:

$$I(t,\xi) = \frac{\sigma}{2}\cos\left(\left[\frac{4\Pi f_0}{c} + \frac{4\Pi(f_1 - f_0)}{cT}\mathrm{t}\right](r_0 + \dot{r}\xi)\right) \quad \text{, and} \tag{25}$$

$$Q(t,\xi) = -\frac{\sigma}{2}\sin\left(\left[\frac{4\Pi f_0}{c} + \frac{4\Pi(f_1 - f_0)}{cT}\mathrm{t}\right](r_0 + \dot{r}\xi)\right). \tag{26}$$

If we sample I and Q we get functions of fast time t and slow time ξ. Therefore, I and Q are two dimensional functions. I and Q vary in fast time t with frequency $\frac{2r_0(f_1 - f_0)}{cT}$ which is proportional to the target range. I and Q also vary with the slow time with frequency $\frac{2\dot{r}f_0}{c}$, which is proportional to the target velocity or range-rate. Now we can perform a 2-dimesional FFT on the analytical signal $F(t,\xi) = I(t,\xi) + iQ(t,\xi)$ and scale the graph axes properly to get an ambiguity function that determines the target range and velocity correctly.

2.5 Relation between Material Refractive Index and Reflectivity of Microwave Signal

Our goal in this thesis is to explore the variation of reflectivity due to material properties. We use a model developed for through-the-wall (TWI) Imaging in THz range [7][8]. The model offers the reflectivity of plain electromagnetic wave from different types of material surfaces in THz frequency range. Our proposed integrated radar-mote includes a K_a band Doppler radar. Therefore, we extend the existing reflectivity model to incorporate Doppler shift and relevant frequency

band in our experimental radar. In this section we explain the existing model while our modified model will be discussed in Chapter 3.

For the existing model [7][8], we consider reflecting materials to be non-conducting for simplicity. Since the materials are assumed to be non-conducting, they have no conductivity and constant permittivity. Therefore, the refractive index is constant and real valued for a specific material type. The authors obtain the reflectivity model equation from planar expansion of the Green's functions and by employing spherical coordinates [8]. We represent the summary of the derivation of the model [8].

Reference 8 obtains a mathematical model to derive a transfer function of a reflecting medium [8]. They assume that the wave propagates into the medium with an index of refraction (n_m).The source of the signal is located at $r_0 = -z_0\hat{z}$ and coordinates are shown in Fig. 7 [8].

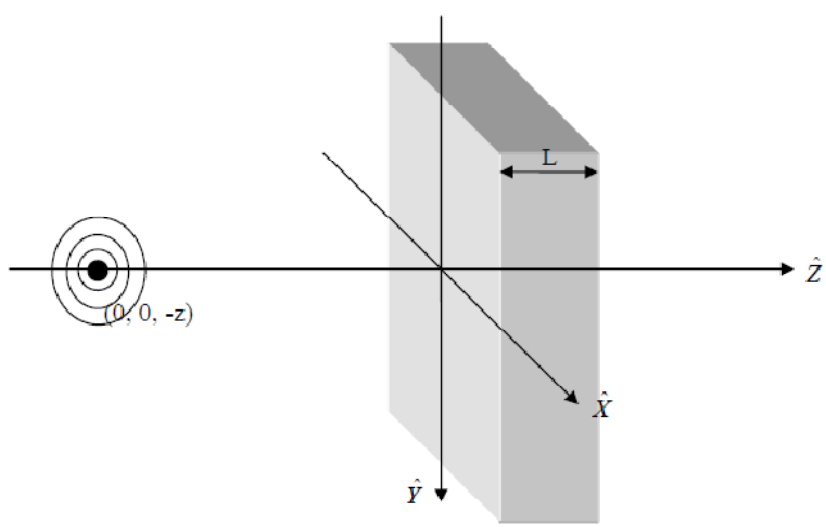

Fig. 7: Wave from a point source through a medium

The wave equation with source $s(r,t)$ in the time domain is as follows

$$\nabla^2 E - \frac{n^2}{c^2}\frac{\partial^2 E}{\partial t^2} = s(r,t). \tag{27}$$

Here, n is the refractive index, c is the speed of light and E is the electric field intensity. Now we express the source terms of angular frequency (ω) and oscillation frequency (v) as follows,

$$s(r,t) = \frac{1}{2\pi}\int_{-\infty}^{\infty} S(r,\omega)e^{i\omega t}d\omega \ . \tag{28}$$

Here, $S(r,\omega)$ is the source angular frequency. Using the well known identity $\omega = 2\pi v$ and $d\omega = 2\pi dv$, we represent Eq. (28) in terms of oscillation in frequency domain as,

$$s(r,t) = \int_{-\infty}^{\infty} S(r,v)\, e^{i2\pi vt}dv \ . \tag{29}$$

Using the solution of the plane wave equation we know a time independent wave equation is given as follows,

$$\nabla^2 E + n^2 k^2 E = S(r,v) \ . \tag{30}$$

Substituting the source at point $r_0 = -z_0\hat{z}$ and using Green's function, Eq. (30) is given as,

$$\left(\nabla^2 + k^2 n^2(z)\right) g(r, r_0) = \delta(r + r_0) = \delta(x)\delta(y)\delta(z + z_0) \ . \qquad (31)$$

Here wave number is $k = {}^{2\pi}/_{\lambda}$ and λ is the wavelength in free space. The refractive index of the system is as follows,

$$n(z) = 1 \ , n, 1 \ , for \ z < 0, 0 =< z =< L, \ L < z \quad resepective \qquad (32)$$

The frequency domain solution for E is given as,

$$E(r, v) = g(r, r_0) S(r, v) d^3 r_0 \qquad (33)$$

where $g(r, r_0)$ is the Green's function in the spatial domain. The time domain solution of E is computed doing the inverse Fourier Transform of Eq. (33)

$$E(r, t) = \int_{-\infty}^{\infty} E(r, v) e^{i2\pi vt} dv \ . \qquad (34)$$

In this work, we assume the materials to be non-conductive, therefore, the electromagnetic wave can propagate the medium with little damping [8]. As we have put the source at $r_0 = -z_0 \hat{z}$ along the $\hat{z}$ direction equation (31) can be converted in Fourier domain as follows,

$$G\left(v_x, v_y, z, r_0\right) \cong \int_{-\infty}^{\infty} \int_{-\infty}^{\infty} g(x, y, z, r_0) e^{-i\left(2\pi v_x x + 2\pi v_y y\right)} dx dy \ . \qquad (35)$$

$$g(x, y, z, r_0) \cong \int_{-\infty}^{\infty} G\left(v_x, v_y, z, r_0\right) e^{i\left(2\pi v_x x + 2\pi v_y y\right)} dv_x dv_y \ . \qquad (36)$$

Now substituting Eq. (36) in equation (31), using the identity in equation (35) and using the wave number definition, we can get homogeneous wave equation given as,

$$\frac{\partial^2}{\partial z^2} G\left(v_x, v_y, z, r_0\right) + [k^2 n^2(z) - |F|^2] G\left(v_x, v_y, z, r_0\right) = 0 \ . \qquad (37)$$

The solution of the Eq. (37) is given as,

$$G\left(v_x, v_y, z, r_0\right) = A e^{iz\sqrt{k^2 n^2(z) - |F|^2}} + B e^{-iz\sqrt{k^2 n^2(z) - |F|^2}} \ . \qquad (38)$$

The two terms in the right side of the equations $A e^{iz\sqrt{k^2 n^2(z) - |F|^2}}$ and $B e^{-iz\sqrt{k^2 n^2(z) - |F|^2}}$ are termed as right going wave and left going wave respectively. As the left going wave is reflected back to the point source, we will follow this one from now on.

The solutions of the wave equations in each region must satisfy the boundary conditions. The boundary condition states that the wave and derivative must be continuous at all boundaries. Then we can compute the coefficients of each component wave as shown in Fig.8.

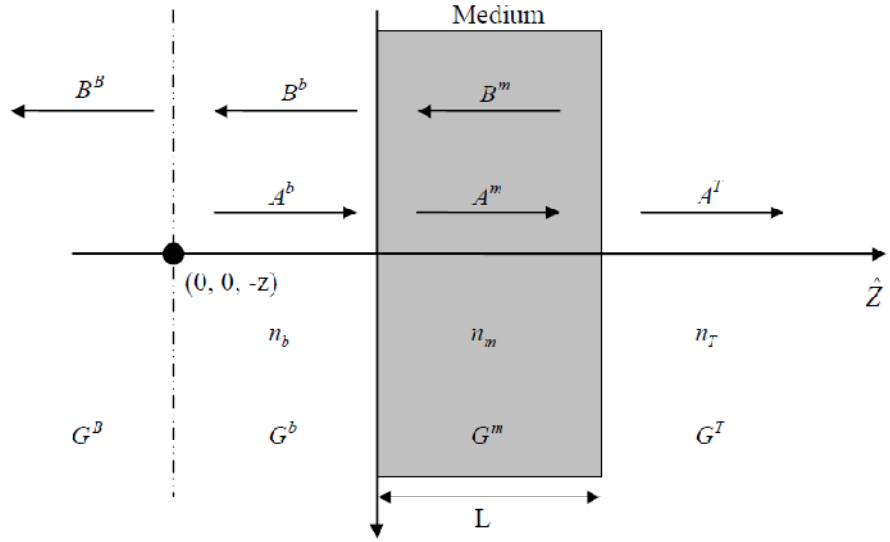

Fig. 8: Cross sectional view of wave front

If the refractive index obeys the following conditions: $n_b(z < 0), n_m(0 =< z =< L)$ and $n_T(L < z)$,we can get the solution for the co-efficient of the Green's function as follows [8],

$$M_1 \begin{bmatrix} A^b \\ B^b \end{bmatrix} = M_2 \begin{bmatrix} A^m \\ B^m \end{bmatrix} \quad . \tag{39}$$

$$M_3 \begin{bmatrix} A^m \\ B^m \end{bmatrix} = M_4 \begin{bmatrix} A^T \\ 0 \end{bmatrix} \quad . \tag{40}$$

$$M_5 \begin{bmatrix} A^b \\ B^b \end{bmatrix} = M_6 \begin{bmatrix} B^B \\ 0 \end{bmatrix} + \begin{bmatrix} 0 \\ 1 \end{bmatrix} \quad . \tag{41}$$

The reflection and transmission amplitudes can be expressed in terms of incident wave A^b as,

$$\begin{bmatrix} A^b \\ B^b \end{bmatrix} = M_1^{-1} M_2 M_3^{-1} M_4 \begin{bmatrix} A^T \\ 0 \end{bmatrix} \quad . \tag{42}$$

A few algebraic simplifications of Eqs. (38) and using Eqs. (39) - (42) yields the reflectance or reflectivity coefficient R =r*r , where

$$r = \frac{B^b}{A^b} = \frac{\left(\sqrt{N_T} + \sqrt{N_m}\right)\left(\sqrt{N_b} - \sqrt{N_m}\right) + \left(-\sqrt{N_T} + \sqrt{N_m}\right)\left(\sqrt{N_b} + \sqrt{N_m}\right)e^{i2L\sqrt{N_m}}}{\left(\sqrt{N_T} + \sqrt{N_m}\right)\left(\sqrt{N_b} + \sqrt{N_m}\right) + \left(-\sqrt{N_b} + \sqrt{N_m}\right)\left(\sqrt{N_T} - \sqrt{N_m}\right)e^{i2L\sqrt{N_m}}} \tag{43}$$

Further algebraic simplification yields the reflectivity of the electromagnetic wave expressed as follows [8]

$$\mathrm{R} = \frac{(\mathrm{N}-\mathrm{N_m})+(\mathrm{N_m}-\mathrm{N})\mathrm{e}^{\mathrm{i2L}\sqrt{\mathrm{N_m}}}}{(\sqrt{\mathrm{N_m}}+\sqrt{\mathrm{N}})^2-(\sqrt{\mathrm{N_m}}-\sqrt{\mathrm{N}})^2\mathrm{e}^{\mathrm{i2L}\sqrt{\mathrm{N_m}}}} \quad . \tag{44}$$

where, $$\sqrt{N_m} = \sqrt{n_m^2 k^2 - (2\pi v_x)^2 - \left(2\pi v_y\right)^2}, \text{ and} \tag{45}$$

$$\sqrt{N} = \sqrt{k^2 - (2\pi v_x)^2 - \left(2\pi v_y\right)^2} \quad . \tag{46}$$

Here, n_m is the refractive index of the reflecting material, k is the wave number and $k = 2\pi f/c$, *c* is the speed of light, $v_x = 1/\lambda_x$ and $v_y = 1/\lambda_y$,and λ is the wavelength of the electromagnetic signal. Now using the spherical coordinate representation we obtain,

$2\pi v_x = k\sin\theta\ \cos\emptyset$, $2\pi v_y = k\sin\theta\ \cos\emptyset$, and $2\pi v_y = k\cos\theta$ (47)

Substituting Eqs. (45) and (46) into equation (47) we get

$$\sqrt{N_m} = k\sqrt{n_m^2 - sin^2\theta},\ \sqrt{N} = k\sqrt{1 - sin^2\theta} = k\cos\theta \quad (48)$$

Now inserting the above results in Eq. (44) we obtain the reflectivity as follows [8],

$$R(\theta) = \frac{(1 - n_m^2) + (n_m^2 - 1)e^{i2kL\sqrt{n_m^2 - sin^2\theta}}}{\left(\sqrt{n_m^2 - sin^2\theta} + \cos\theta\right)^2 - \left(\sqrt{n_m^2 - sin^2\theta} - \cos\theta\right)^2 e^{i2kL\sqrt{n_m^2 - sin^2\theta}}}. \quad (49)$$

If we consider the incident wave angle θ=0, then equation (49) yields

$$R = \frac{(1-n_m^2)+(n_m^2-1)e^{i2kn_mL}}{(n_m+1)^2-(n_m-1)^2e^{i2kn_mL}} \quad (50)$$

2.6 Power Spectrum Analysis with Multiple Signal Classification (MUSIC) Technique

Multiple Signal Classification (MUSIC) is a widely accepted power spectrum estimation algorithm. The MUSIC technique has been widely used telecommunication, biomedical, signal processing and electromagnetic disciplines to solve problems such as spectrum and signal estimation, the

direction of arrival [33]-[37]. The MUSIC algorithm estimates the Pseudospectrum of a signal using Schmidt's eigenspace analysis method [31]. The MUSIC algorithm produces a spectral estimate of a signal performing the eigenvector-eigenvalue decomposition of the autocorrelation matrix of the signal [32]. The MUSIC spectral estimate is represented as follows,

$$P_{MUSIC}(f) = \frac{1}{e^H(f)\left(\sum_{k=p+1}^{N} v_k v_k^H\right)e(f)} = \frac{1}{\sum_{k=p+1}^{N} \left|v_k^H e(f)\right|^2} \quad , \qquad (51)$$

where N is the dimension of the eigenvectors, v_k is the k-th eigenvector, and integer p is the dimension of the signal subspace. The vector e(f) consists of complex exponentials, so the inner product $v_k^H e(f)$ amounts to a Fourier transform which is used to compute the Pseudospectrum estimate. The Pseudospectrum estimate is computed by computing FFT for each v_k and summing their squared magnitudes.

The MUSIC algorithm is used for extracting MUSIC Spectrum Matrix (MSM).It is a parametric spectra estimation method which manipulates the fact that the sinusoidal signal components making up a transient signal and the added gaussian noise are correlated [37].Let us assume that [37],

$$y(n) = x(n) + \omega(n) = \sum_{i=1}^{L} c_i\, e^{s_i n} + \omega(n), \qquad \mathrm{n} = 1,2,\ldots,\mathrm{N}$$

(52)

represents the scattered signal of a given target recorded at certain aspect combination and sampled at total of N discrete time points in presence of additive gaussian noise ω(n).Here x(n) is the noise free signal component expressed in terms of linear combination of L complex exponentials with target poles s_i, where i=1,2,….,L. The term c_i in Eq. (52) is complex valued weight co-efficients. For an integer m which satisfies the condition L < m < N, the vector y (n) can be formed as [37],

$$y(n) = [z(n) \;\; z(n-1) \ldots \quad z(n-m+1)]^T \tag{53}$$

The correlation matrix of the vector can be expressed as

$$IR = E\{y(n)y(n)^H\} = ACA^H + \sigma^2 I_{M\times M} \quad , \tag{54}$$

Where, E is the expected value operator denotes complex conjugate transpose, σ^2 is the variance of Gaussian noise, I is the unit matrix and

$$A = [a(s_1) \quad a(s_2) \quad \ldots \quad a(s_L)] \tag{55}$$

$$a(s) = \left[1 \quad e^{-s} \;\ldots. \quad e^{-s(m-1)}\;\right]^T \tag{56}$$

Let $\lambda_1 \geq \lambda_2 \geq \cdots \geq \lambda_2$ be the eigenvalues of the correlation matrix IR,$\{e_1 e_2, \ldots, e_L e_{L+1}, \ldots, e_m\}$ be the set of corresponding orthonormal eigenvectors, and $G = [e_{L+1} \ldots\ldots e_m]$ be the eigenvector matrix corresponding to these eigenvalues. Then the MUSIC spectrum function can defined as follows,

$$P_{MUSIC}(s) = \frac{1}{a^H G G^H a(s)}, \quad (57)$$

where $s = \alpha + j\omega$ is the complex frequency. The function has peak values at $s = s_i$ and can be approximated by a matrix known as MUSIC spectrum matrix.

In this thesis, MUSIC algorithm is used as a signal processing tool to extract target feature for classification of materials target are made of. We use the MUSIC algorithm as the fundamental signal processing tool to extract feature matrix or MUSIC Spectrum matrix (MSM) for each type of target. We use the "pmusic" function available in MATLAB toolbox to get the power spectrum of each radar signals. Figure 9 shows a sample spectrum output of a signal vector via MUSIC. The steps from feature extraction to classification are discussed in Chapter 3.

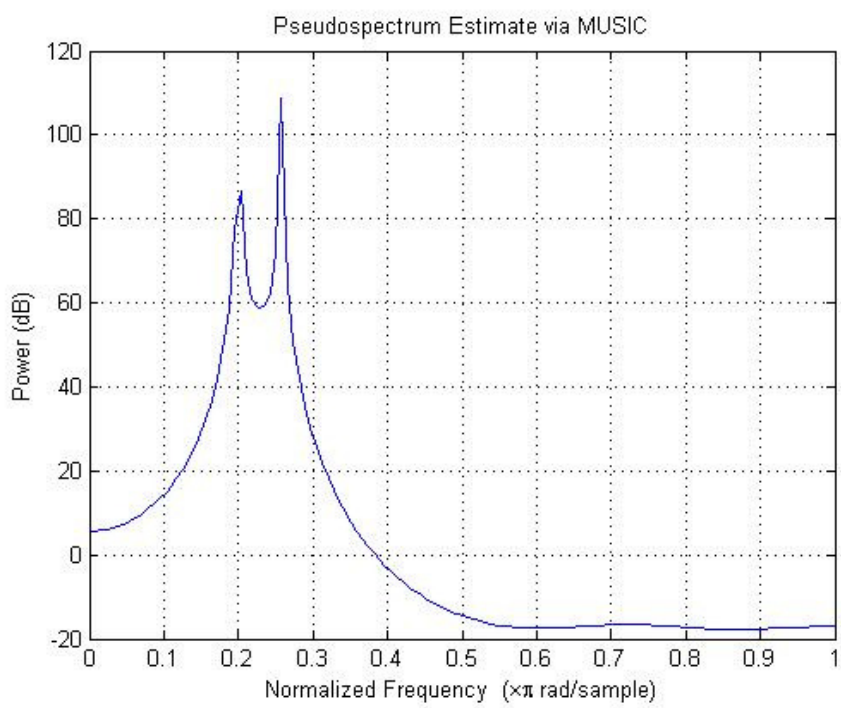

Fig. 9: Power spectrum of signal vector via pmusic

2.7 WEKA Machine Learning Tool and Classification

We use WEKA (Waikato Environment for Knowledge Analysis), a popular suite of machine learning software, for analyzing the data collected through integrated radar-mote experiments. This section provides an overview of the WEKA tool.

2.7.1 WEKA Overview

The Weka is written in Java, and is developed at the University of Waikato, New Zealand. It is free software available under the GNU General Public License [38][39]. The machine learning algorithms available in WEKA can either be applied directly to data using the WEKA Graphical User Interface (GUI) or user java program by calling the WEKA library. We use the WEKA GUI explorer to analyze the data collected through our experimental system. The WEKA GUI provides a starting point for launching WEKA's main GUI applications and supporting tools. The GUI consists of four buttons, one for each of the four major WEKA applications and four menus [39].The four applications related to four buttons are Explorer, Experimenter, KnowledgeFlow and SimpleCLI. WEKA Explorer is the software environment for testing data with machine learning process. We use this tool for our data analysis. Therefore, we provide the details of this tool skipping other three in following sections.

2.7.2 How to use WEKA?

The WEKA explorer has tools for exploring different data manipulation tasks such as data preprocessing, classification, regression, clustering, association rules, and visualization. We use data preprocessing and classification for our data

manipulation. The data preprocessing tool has different types of data filters such as Principal Component Analysis (PCA), Normalization etc. The classification tool includes different types of classifiers such as naïve bayes classifier, support vector machine, multi layer perceptron, random forest and many more. We provide a brief overview of the classifiers we use in the following section. The function of WEKA in case of our data analysis is explained in Fig.10. The raw data collected from experiment is fed to the WEKA toolbox with the desired data format required. Then WEKA performs the preprocessing and classification to produce output in a specific format. The data processing is briefly discussed below,

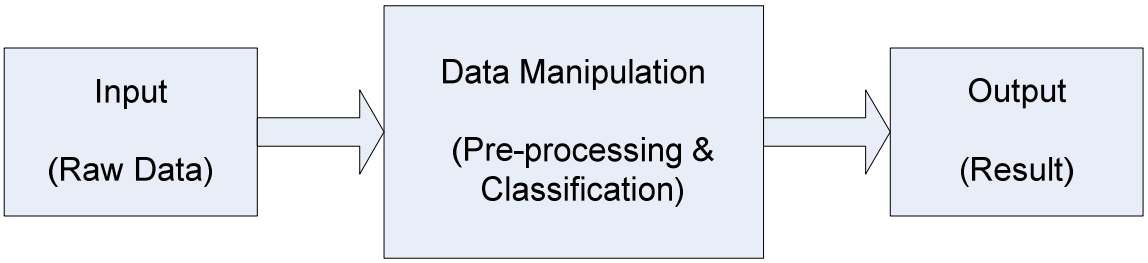

Fig. 10: Function of WEKA Machine Learning Tool

Suppose each column of data represents one attribute and each row represents an instance of a class. We need to classify them. Typically these types of data are stored in a spreadsheet and database. However, WEKA expects the data in a specific format named as Attribute Relation File Format (ARFF). It is necessary to have type information about each attribute which cannot be automatically deduced from the attribute values. Therefore, the data must be must be converted to ARFF form before any algorithm is applied to the data set [40]. Most

of the spreadsheet and database software allow saving data in Comma Separated Values (CSV) format. The WEKA has tool to convert the CSV format data to ARFF format. In our work we plan to save the experimental data in CSV format.

2.7.3 Understanding WEKA Output

WEKA classification output offers performance measure of the classifier in different matrix. A few performance measures of WEKA output such as “Correctly Classifier Instances” are self-evident while some others such as “kappa statistic”, “confusion matrix” requires explanation. This section gives a brief overview of the different performance measures shown in WEKA output.

Accuracy of the classifier is given in percentage as output. The accuracy can be represented as,

$$Accuracy = \frac{number\ of\ correctly\ classified\ instances}{total\ number\ of\ instances}, \tag{58}$$

For any classifier precision and recall can be expressed as follows,

$$precision(A) = \frac{number\ of\ correctly\ classified\ instances\ of\ class\ A}{number\ of\ instances\ classified\ as\ belonging\ to\ class\ A}, \tag{59}$$

and

$$recall(A) = \frac{number\ of\ correctly\ classified\ instances\ of\ class\ A}{number\ of\ instances\ in\ class\ A}. \tag{60}$$

Confusion matrix shows an overall picture of the performance showing the distribution of correctly and incorrectly classified instances. Figure 11 shows a typical confusion matrix given by WEKA output after applying a classifier to a sample data.

```
=== Confusion Matrix ===

 a b   <-- classified as
 7 2 | a = yes
 3 2 | b = no
```

Fig. 11: Confusion matrix from WEKA Classification Result with J48 classifier for the weather data.

WEKA attempts to classify instances into two possible classes labeled as “yes” or “no”. However, for user convenience WEKA substitutes the classes with letters ‘a’, ‘b’ respectively. The first column of the confusion matrix shows that in total 10 instances are classified as ‘a’ and the second column shows that 4 instances are classified as ‘b’. The rows show the actual number of instances under class ‘a’ and ‘b’. It also represents, how many instances are correctly and incorrectly classified. For instance, from the confusion matrix we can say that 7 of the

instances are correctly classified as ‘a’ whereas 2 were incorrectly classified as ‘b’.Similar observation is evident for row two.

ROC curve is a plot of the true positive rate against the false positive rate for the different possible cut points of a diagnostic test. It shows the tradeoff between sensitivity and specificity. The area under the curve is a measure of test accuracy. Kappa statistic measures the agreement of predictions with the actual class. In general, Kappa statistics are only appropriate for testing whether agreement exceeds chance levels, i.e. that predictions and actual classes are correlated. True positive rate is equivalent to the term “recall”. False positive can be represented as follows,

$$False\ Positive(A) = \frac{number\ of instances\ \ incorrectly\ classified\ as\ class\ A}{total\ number\ of\ instances\ except\ \ class\ A}, \tag{61}$$

F-measure is a combined measure of precision and recall. F-measure is represented as ,

$$F - measure = \frac{2 * precision * recall}{precision + recall}. \tag{62}$$

2.7.4 WEKA Classifiers overview

WEKA provides the implementations of state-of-the-art learning algorithms. One can preprocess a dataset, feed it into a learning scheme, and analyze the resulting classifier and its performance [40]. The learning schemes are called classifiers in WEKA. Here, we give a brief overview of the classifiers we use in our work.

J48

J48 is an open source java implementation of the C4.5 machine learning algorithm in WEKA. C4.5 is an algorithm used to generate a decision tree developed by Ross Quinlan [42]. As the decision trees generated by C4.5 can be used for classification, C4.5 is often referred to as a statistical classifier [43]. The C4.5 algorithm builds decision tree from a set of training data using information entropy. Suppose we have a training set $S= s_1,s_2,s_3, \ldots$..from already classified samples. Now each sample $s_i= x_1,x_2,x_3,\ldots$ is considered a vector where $x_1,x_2,x_3, \ldots$ represents attributes or features of the sample. The training data is then augmented with a vector $C=c_1,c_2,c_3,\ldots$ where $c_1,c_2,c_3,\ldots$ represents the class to which the samples belong. For each node of the tree the algorithm picks one attribute of the data that most effectively splits its set of samples into subsets enriched in one class or other. The criterion to pick is the normalized information gain or difference in entropy that results from choosing an attribute for splitting data. The attribute which has the highest information gain is chosen to make decision. The decision tree algorithm then recurs on the smaller sub lists [43].

Support Vector Machines

Support Vector Machines (SVMs) are a set of supervised learning methods used for classification and regression analysis. The standard SVM is a non-probabilistic binary linear classifier. For a given input it predicts which of the two possible classes the input belong to. An SVM is a model representation of example points mapped in space such a way that examples in different categories are divided in clear gap. In formal notion, we can say that the SVM creates hyperplane or a set of hyperplanes in high dimensional space that can be used for classification or regression analysis [44].

Suppose we are given a training data set D with n points [44],

$$D = \{(X_i, c_i) | X_i \epsilon R^p, c_i \epsilon \{-1,1\}\}_{i=1}^{n} \quad . \tag{57}$$

Here, c_i is either -1 or 1 and they indicate which class the point X_i belongs. Each X_i is a p dimensional real vector. Our target is to find maximum-margin hyperplane that divides points having the value of $c_i = -1$ from $c_i = 1$ .The hyperplane equation satisfying each X is as follows,

$$w.X - b = 0 \quad . \tag{58}$$

Here, . stands for dot product, w is a normal vector perpendicular to the hyperplane and $\frac{b}{||w||}$ is the parameter that determines offset of the hyperplane from the origin along the vector w.

Now our target is to choose w and b such that the margin is maximum or the distances between parallel hyperplanes are as far apart as possible. This ensures separation between data. The hyperplanes are represented with following Eqs.

$$w.X - b = 1\,, \tag{59}$$

and

$$w.X - b = -1\,. \tag{60}$$

Multiclass SVM assigns labels to instances by using support vector machines, where the labels are drawn from a finite set of several elements. The usual approach in multiclass SVM is to reduce the single multiclass problem into binary classification problem [44].

Random Forest

Random forest is an ensemble classifier. It consists of many decision trees and outputs the class that is the mode of the class's output by individual trees. Leo Breiman and Adele Cutler are given credit for introducing the random forest algorithm [44][45]. Each tree in random forest is constructed using the following algorithm [45],

1. Let the number of training cases be *N*, and the number of variables in the classifier be *M*.

2. We are told the number *m* of input variables to be used to determine the decision at a node of the tree; *m* should be much less than *M*.

3. Choose a training set for this tree by choosing *N* times with replacement from all *N* available training cases. Use the rest of the cases to estimate the error of the tree by predicting their classes.

4. For each node of the tree, randomly choose *m* variables on which to base the decision at that node. Calculate the best split based on these m variables in the training set.

5. Each tree is fully grown and not pruned.

The random forest provides advantages such as handles large number of input variables, produces highly accurate classifier for many data sets, estimates importance of variables in determining classification. It is good for estimating missing data also and maintains good accuracy when portion of data is missing. However, random forest is prone to over fitting in some cases [45].

Multilayer Perceptron

Multilayer perceptrons (MLPs) are feed forward neural networks which are trained with the standard back propagation algorithm. MLP consists of multiple layers of nodes in a directed graph that is fully connected from one layer to the next. Except for the input nodes, each node is a neuron or processing element with a nonlinear activation function. MLP utilizes a supervised learning technique called back propagation for training the network. WEKA has a MLP implemented in it. As MLPs are supervised networks those need to be trained to obtain desired response. MLPs learn to transform input data into a desired response. Therefore,

they are widely used for pattern classification. MLPs can approximate virtually any input-output map with one or two hidden layers [46]-[48].

In MLP, an external input vector is supplied to the network by clamping it at nodes in the input layer. For conventional classification problems the appropriate node is clamped to 1 state during training while the others are clamped to 0 [48].Consider the graph in Fig.12.

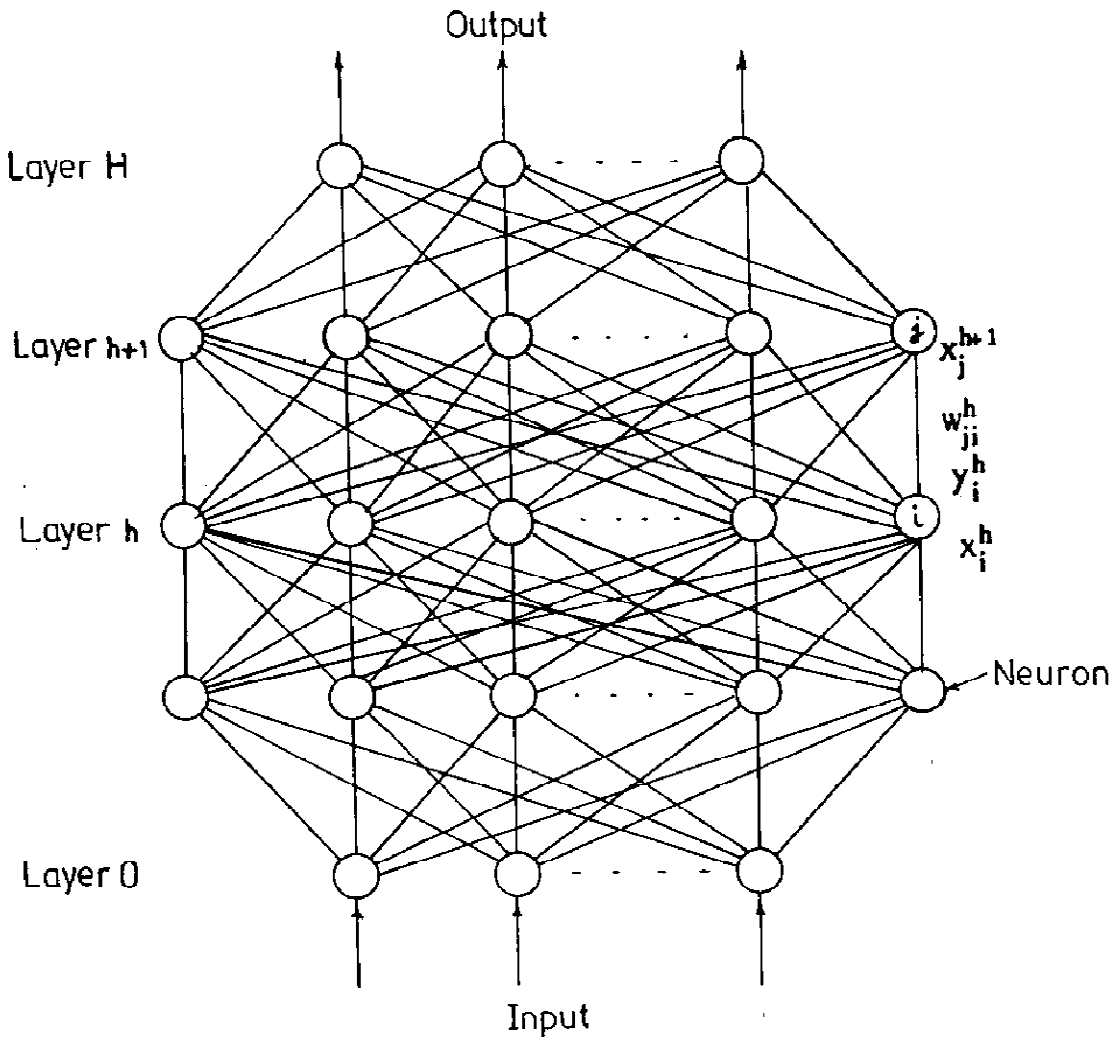

Fig. 12: A neural network with 3 hidden layers. (Source: Ref.48)

The total input x_j^{h+1}, received by neuron j in layer $h+1$ is defined as [48],

$$x_j^{h+1} = \sum_i y_i^h w_{ji}^h - \theta_j^{h+1}, \tag{61}$$

Where y_i^h is the state of *i*-th neuron in preceding h-th layer, w_{ji}^h is the weight of the connections from *i*-th neuron in layer h to *j*-th neuron in layer $h+1$,and θ_j^{h+1} is the threshold of the *j*-th neuron in layer $h+1$.The output of a neuron in any layer other than input layer is a monotonic nonlinear function of its inputs and given by following Eq. [48],

$$y_j^h = \frac{1}{1+e^{-x_j^h}} \tag{62}$$

The learning procedure needs to determine the internal parameters of the hidden layers based on its knowledge of inputs and desired outputs. The procedure continues until the states of the neuron in output layers H are determined.

Rotation Forest

Rotation Forest is an ensemble of classifier which can do classification and regression depending on a base learner. This is a method for generating classifier ensembles based on feature extraction. The feature set is randomly split into K subsets to create training data for a base classifier. Then Principal Component Analysis (PCA) is applied to each of the subsets. All principal components are retained in the ensemble to preserve the variability information

in the data. Now, K axis rotations are performed to form new features for a base classifier. The main theme of the rotation strategy is to encourage individual accuracy and diversity within the ensemble simultaneously [49].

Combination of Classifiers

WEKA provides methods for combining different classifiers. Different combinations of probability estimates can be used for combination rules. For instance the combination classifier may decide based on the average of probabilities, product of probabilities, majority voting, median of member classifiers [50]. Vote and Stacking are two commonly used classifiers to combine different base classifiers.

In Chapter 3, we discuss detail design and implementation of integrated radar-mote. Our goal is to develop an integrated sensor system with commercially available low-cost devices which can be used as an effective sensor network system for surveillance and tracking in complex scenario. Although our system is not conceptually different from the system described in section 2.1, however, it is built with cheap and COTS components. Our system is different from implementation and application perspective also. For instance, the radar used in our integrated radar-mote offers more capabilities than other existing systems. We provide the detail description of the components will be provided in next Chapter 3. We also we perform experiments with the prototype autonomous radar-mote system and other commercial sensor boards to explore the capability of the experimental system for surveillance and tracking application.

Chapter 3

Proposed Design and Methods

This chapter discusses the contribution of this thesis. At first, we present the design and implementation of our proposed integrated radar-mote sensor system. The design includes the hardware and software level modification required to incorporate a Doppler radar into the wireless sensor network system. A modified version of the reflectivity model based on the model explained in Background review Chapter 2 is proposed. The simulation of electromagnetic signal based on modified model is followed by discussion of the model. Finally, we propose the steps of classifying a few non-conducting target using MUSIC signal processing technique as feature extraction tool.

3.1 Radar-Mote Integration

The Doppler radar system and the wireless mote work individually as separate and stand-alone sensor systems. The systems have their own advantages as well as limitations. We integrate these two sensor systems to work as a single sensor network system to improved sensing and target tracking capabilities.

3.1.1 Standalone Miniature Doppler Radar System

In this section we discuss the miniature Doppler radar prior to integration with the TelosB mote. The miniature Doppler Radar system requires more human intervention to operate. Figure 13 shows the miniature Doppler radar system with the peripheral component connections before integration. The components of the

Doppler radar system include Miniature Doppler radar, DC power supply, Function generator, and Storage oscilloscope.

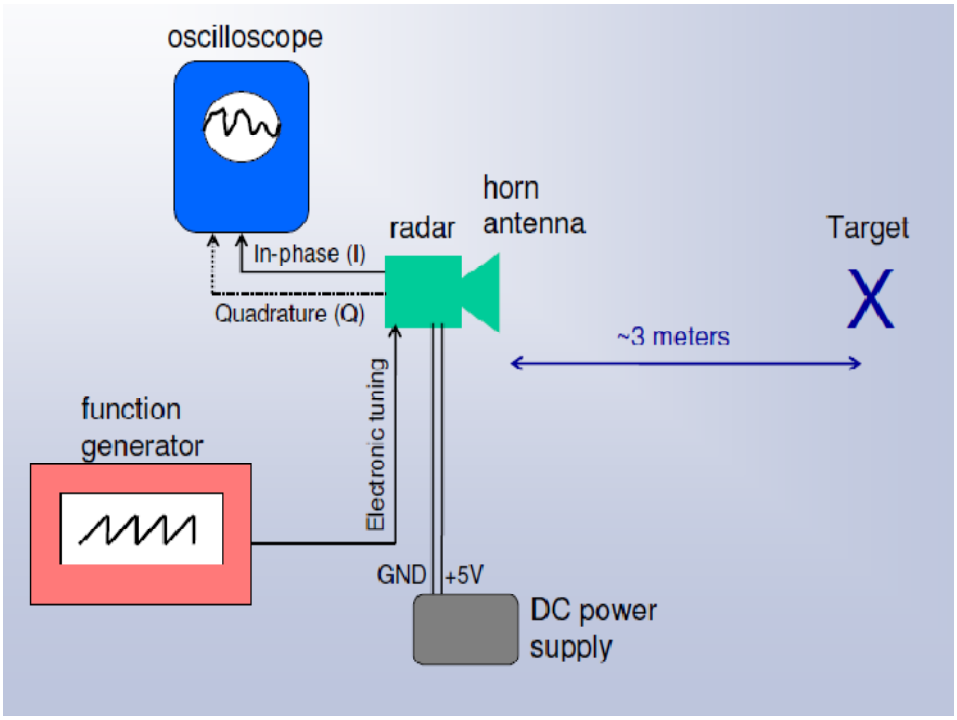

Fig. 13: Radar System before Integration

The miniature Doppler radar has the following five pins : DC power source and ground pins, voltage tuning Input pin, and two output pins (In-Phase and Quadrature). The DC power source provides the 5V required for Doppler transceiver operation. The function generator provides a ramp signal of fixed voltage (0.3 to 5V) and frequency (1 KHz). The output of the radar signal at any instant can be expressed as a function of the target range and velocity. The detail description about Doppler radar is provided in Chapter 2.of Equation (25) gives the mathematical relation of the I-Channel radar output.

3.1.2 Wireless Mote before Integration

Note a more detail discussion on the wireless Mote is found in Chapter 2. In this section we provide a brief overview of the standalone wireless mote. We use TelosB mote platform for our system. WiEye and SBT80 sensor boards are plugged into the TelosB mote. Figure14 shows a typical setup of the wireless network system before integration.

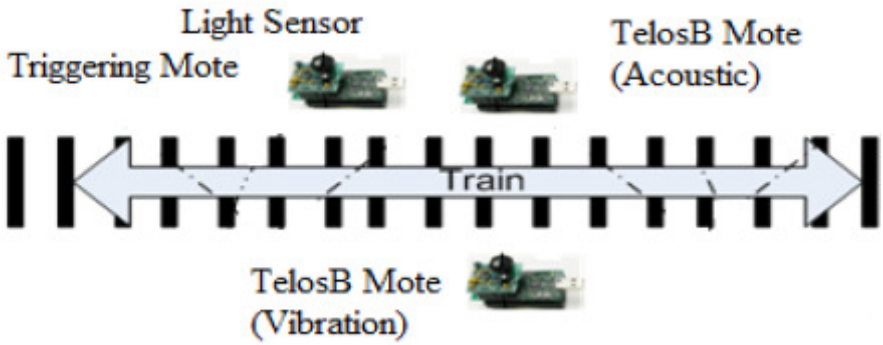

Fig. 14: Wireless Mote before integration

Figure 14 shows a toy train track, two WiEye sensor board plugged into TelosB mote, and a SBT80 sensor plugged into TelosB mote. WiEye sensor board has passive infrared (PIR), visual light, and acoustic sensor [51]. SBT80 has 8 sensors such as visual light, infrared, acoustic, temperature, magnetometer, and vibration [52]. We have use acoustics and vibration sensors for our experiment. When the toy train comes within the field of PIR sensor it senses the event and sends a triggering signal to the SBT80 sensor mote. The SBT80 sensor mote senses the acoustic and vibration signals produced by the toy train. The wireless

mote can store the captured signal in the flash disk available with it or transmit it to a base station mote via wireless channels. The wireless motes can operate with little human guidance after deployment. However, wireless motes lack a powerful active sensor such as radar. Therefore, our target is to integrate the Doppler radar with the wireless mote for complementary benefits. In the integrated system wireless mote will add a powerful sensing unit whereas Doppler radar can minimize human intervention in its operation.

3.1.3 Designing of Autonomous and Integrated Sensor System

This section provides a detail design of the proposed integrated sensor. In general, standard wireless sensor mote platform is equipped with different types of built-in passive sensors such as light, temperature, vibration etc.The standard mote platform also supports the extension of the sensor modalities by allowing plug in of specific sensor circuit board using the standard expansion ports of the mote. For example WiEye and SBT80 built by Easysen are two standard sensor circuit boards which can work with TelosB through its expansion ports [51][52]. Our miniature Doppler radar has output pin which produces analog output signal. We plan to connect output pin of the miniature Doppler radar to the input pin of TelosB in our integrated autonomous sensor suite.

3.1.3.1 Steps of Integrating Doppler Radar and Wireless Mote

The first step of the integration is the hardware level integration of the Doppler radar and wireless mote. We connect the output pin of the Doppler radar to one

of the input pins of the TelosB mote. Figure 15 shows the initial schematic diagram of the integrated system.

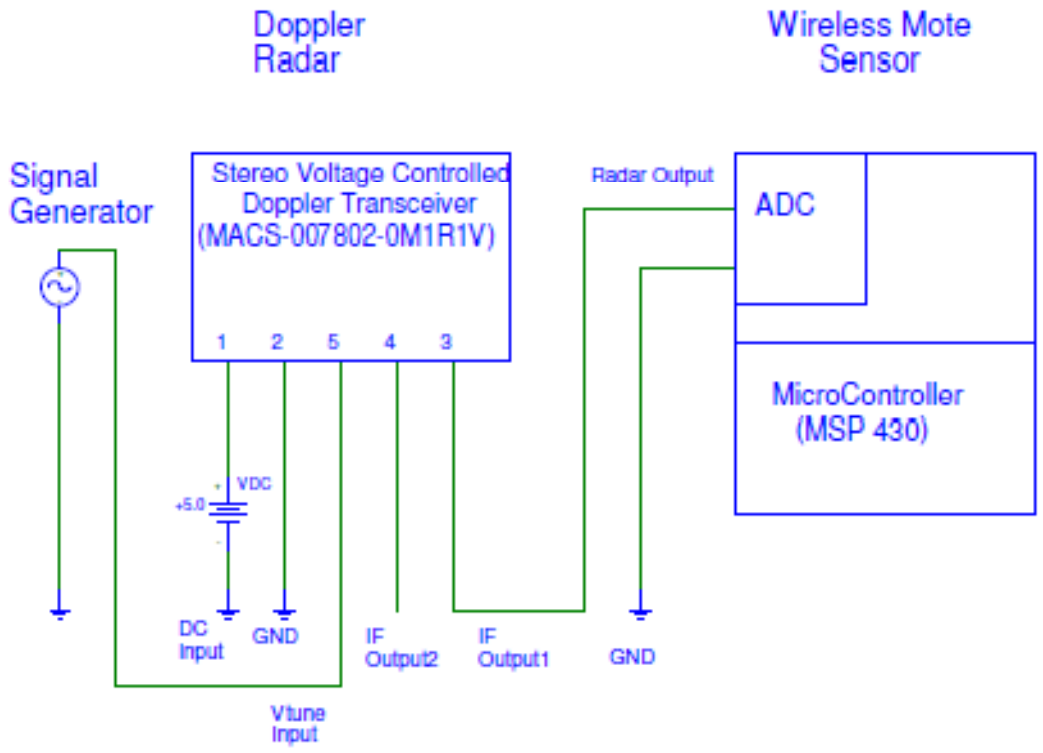

Fig. 15: Initial Design of the integrated Radar-mote system

The next step of the integration is a software level integration. We replace the data capturing task using oscilloscope with that of the TelosB mote. Specifically, the goal is to capture the radar output data using wireless mote. Therefore, this step requires connecting analog radar output as analog input of the already available ADC of the TelosB and sampling the analog signal using the ADC12 with the help of a user program stored in the mote.

We modify a user program which can sample the analog signal with different sampling speeds by changing the program parameters. The sampled analog

signal is then converted to digital signal using the conversion formula in Eq. (1). We select the V_{R+} equals to 1.5V and V_{R-} equals to zero, such that the formula in our case is simplified as follows,

$$V_{ADC} = 4096 * \frac{V_{in}}{V_{R+}} \quad , 0 < V_{in} < 1.5V \tag{63}$$

where the maximum value of V_{R+} can be either 1.5V or 2.5V as the ADC available in mote supports voltage these two maximum levels. Therefore, the ADC supports two ranges of voltage levels from zero to 1.5 or zero to 2.5V. The digital value for the analog voltages ranges from zero to 4096. Here 4096 is the maximum discrete value available.

Before TelosB starts digitizing the radar signal, we need to connect the Doppler radar output to the TelosB mote input as shown in Fig.13.We then load the user program (RadarInputReadStream) into the sensing radar-mote. We also have a base station TelosB mote connected to a workstation via USB port. A user program is also loaded into the base station mote to manage the wireless connection between the sensing mote and the workstation. We also have a data collection program RadarMesseageReader running in the workstation for storing data collected through base station mainly. We can trigger the sensing mote with an ACTIVATE signal from the workstation to the sensing mote via base station. Figure 16 shows the basic steps performed by the user program (RadarInputReadStream) in TelosB from digitizing the analog radar output to sending it to the base station.

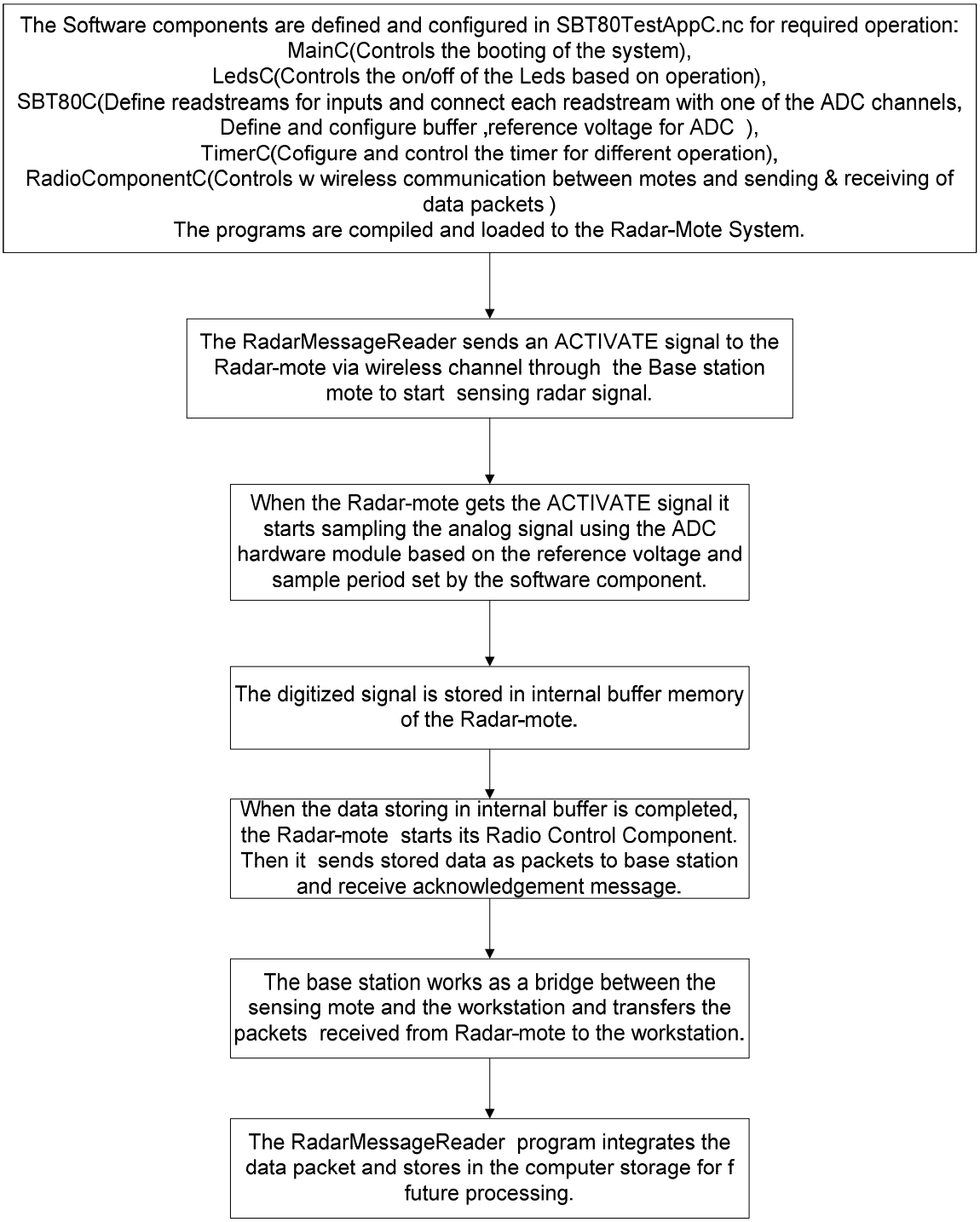

Fig. 16: Flowchart of digitizing the Radar output with wireless mote

Our user program defines and configures the components and modules required for the desired operation of digitizing an analog signal and sending it to a base station wireless mote. The program is written in nesC standard and compiled and loaded before operation. When the radar output is connected to one of the input ports the user program samples the analog program based on the reference voltage and sampling period configured earlier. The digitized data is stored in internal flash buffer. The wireless control module is started to initialize the process of sending the data to the base station. The wireless control module sends the data as small packets maintaining the standard wireless protocols.

Our goal is to build an autonomous radar-mote system which can collect the data from field and send it to a host computer placed in a secure place. The host computer has more processing capability and memory compared to the tiny wireless motes. Therefore, we use the radar-mote only as a data gathering and broadcasting system. The host computer through base station can store the sensed data from a remote sensor mote and analyze the field data to make intelligent decision based on a high level decision support system. Thus, we designed the system where the integrated radar-mote is not directly connected to host computer rather connected to a distant host computer via base station wireless mote. The connections of the stereo Doppler transceiver is same as we discussed in the section 3.1.1.The only difference is that we connect the radar output to one of the input channels of the TelosB mote instead of connecting to the probe of a storage oscilloscope.

3.1.3.2 Initial Design and Test

We perform a series of baseline experiments using the initial integrated system as shown in Fig.15. From our knowledge of experimenting with Doppler radar with different moving targets we find that radar output voltage is typically ranges between 0 to 200mV.We generate analog signal with voltage output similar to Doppler radar using the standard lab signal generator. The signal generator output is connected to the mote as ADC input. Fig. 17 shows the test setup with signal generator.

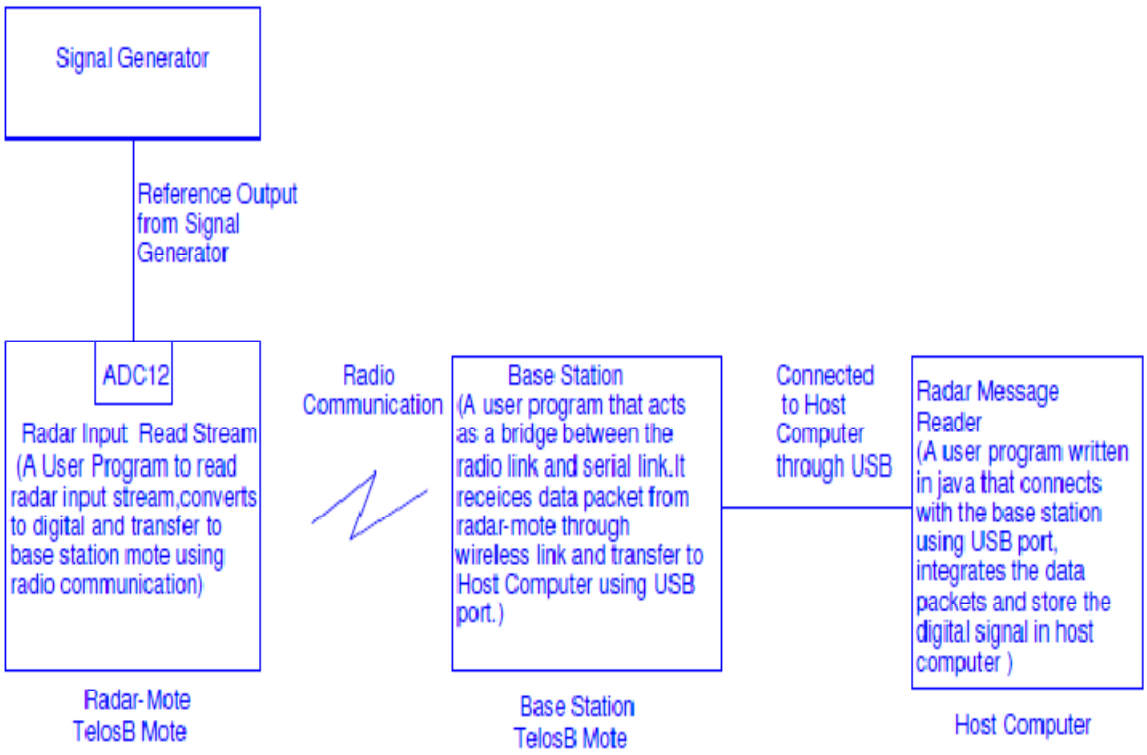

Fig. 17: Test setup flow diagram for data capturing with wireless mote

The signal generator is used to generate reference output signal for test purpose. The signal generator output is connected to one of the input pins of the TelosB mote. The input pin is internally connected to the ADC12 module of the radar-mote [21]. We load the user programs as discussed in section 3.1.3.1.

We successfully sample the analog signal wave (ramp wave) generated by signal generator with maximum sampling rate of 200 KHz using our user program and TelosB mote. The data from radar-mote is sent to the base station and stored in host computer. We then reconstruct the analog signal in host computer and compare with the analog signal captured through storage oscilloscope. Comparison of data captured the by the oscilloscope and the radar-mote shows that these two signals are same. The ramp signals in the following Figs.18 and 19 are captured through oscilloscope and wireless motes respectively. While using the stand alone radar system, the storage oscilloscope samples the signal at a rate of 200 KHz. At 200 KHz sampling rate, the resulting radar signal is good since the data have good resolution. Therefore, we try to use same sampling rate for sampling the analog signal with the radar-mote. Figures 18 and 19 show the ramp signals captured with 200 KHz sampling rate by oscilloscope and wireless mote respectively.

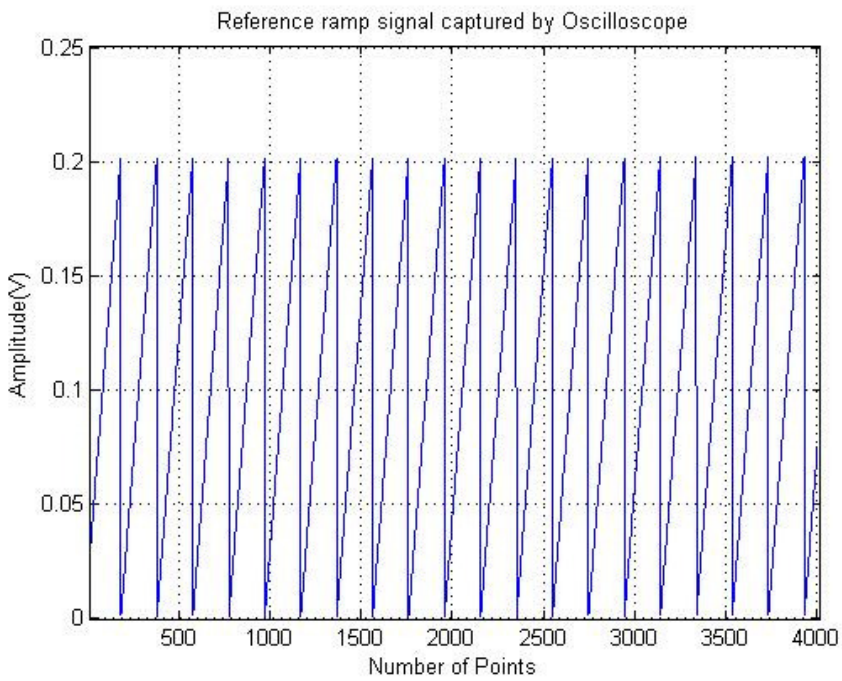

Fig. 18: Ramp signal captured using Storage Oscilloscope with sampling frequency of 200 KHz and peak to peak voltage 200mV

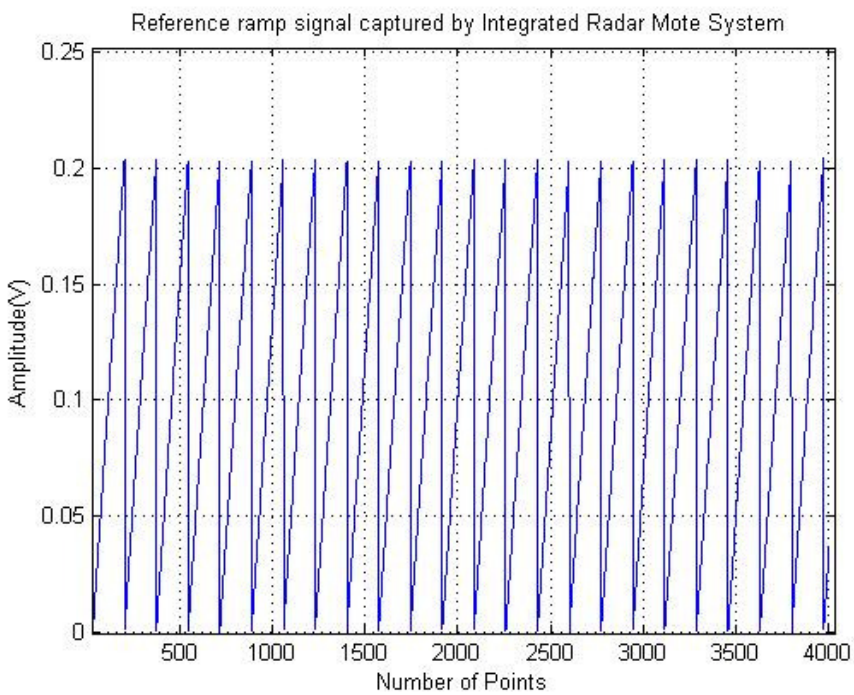

Fig. 19: Ramp signal captured and reconstructed using wireless mote with sampling frequency of 200 KHz and peak to peak voltage 200mV

We then connect the radar output to one of the output pins of the TelosB mote as shown in Fig. 20 and store the radar output to a host computer through radar-mote and base station mote. Figure 20 shows our initial design of data collection using the autonomous radar-mote system.

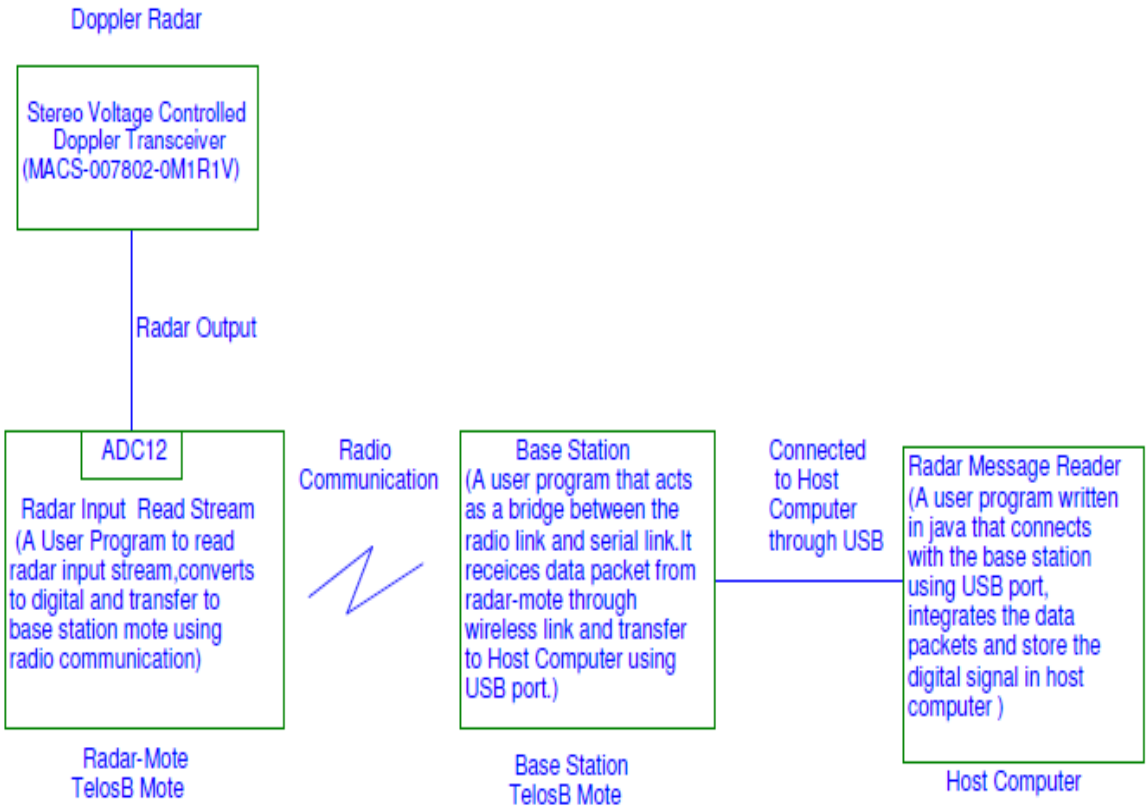

Fig. 20: Initial setup of Experimental autonomous radar-mote wireless network system for data collection.

Note the experimental setup in Fig.20 is almost similar to Fig.17. However, the signal generator is replaced with the Doppler radar system in Fig. 20. TelosB

mote samples the radar signal, converts to digital and sends the digital data to the base station. We have a user program loaded in the base station mote to listen for any data output from the distant motes and to transfer the received data packets to the host computer. The host computer reconstructs captured sample signal. When we capture our signal using the signal generator as input device as shown in Fig.17, we obtain desired ramp output signal as shown in Fig.19. However, when we repeat the experiment with the radar as signal generating device as shown in Fig.20, we do not obtain any output signal in TelosB mote. We had to solve this problem exploring different solutions and testing many times. The final solution is discussed in next section. In principle the radar output signal should have been captured by the radar-mote the same way it works for signal generator output.

3.1.3.3 Solving the problem of Initial Design and Final Design

Upon research on using standard signal generator equipment and Doppler transceivers as input devices we note that the problem is caused due to the difference of output impedance between these two different devices. Standard lab equipment such as signal generators or oscilloscopes has high output impedance. Therefore, even signal with small output voltage like 100mV/200mV from signal generator can drive the input pin of the ADC of the TelosB mote. However, the radar does not have enough power to drive the input pin of the ADC. We solve the problem by designing a voltage follower circuit between the radar output pin and the ADC input pin of the mote as shown in Fig. 21. The voltage follower circuit works as a unity gain amplifier and analog buffer

for the radar output .The voltage follower circuit eliminates the loading effect and works as a required separation between two devices. Figure 22 show the final design and implementation of our radar-mote sensor system.

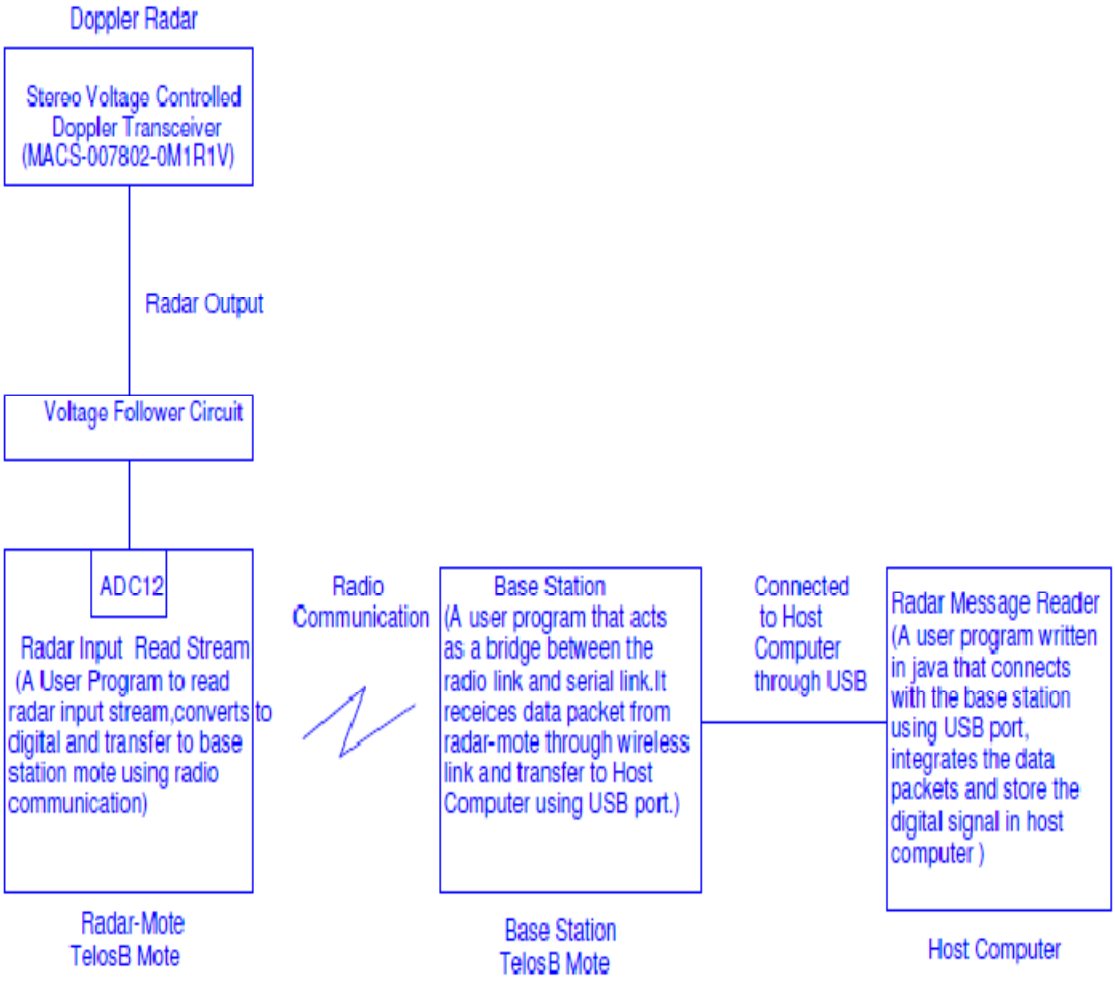

Fig. 21: Final Setup flow diagram of autonomous radar-mote wireless network system for data collection.

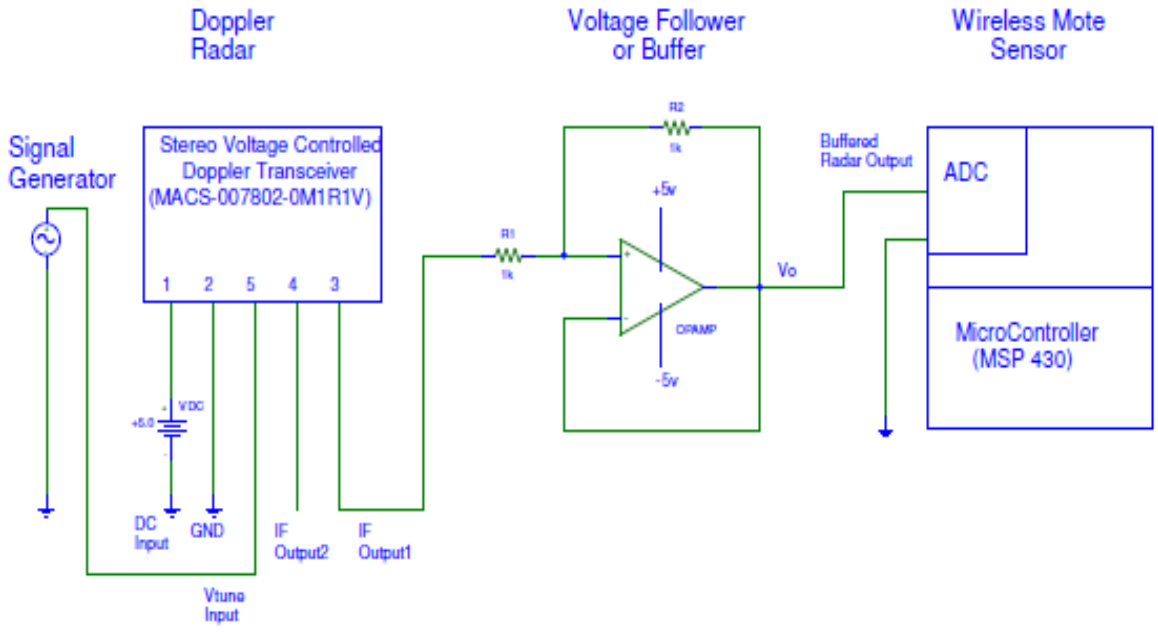

Fig. 22: Final circuit diagram for integration of Doppler radar and wireless sensor platform.

3.1.3.4 Integrated Radar-Mote Sensor Data Collection and Processing

In this section we present the test data collection using our integrated radar-mote system as shown in Fig.22. We store the radar output in comma separated value (csv) format in host computer. The stored data contains sampled digital value of the analog radar signal. We can obtain corresponding digital signal using the ADC conversion formula in Eq. (63). Figure 23 shows an example radar signal captured and reconstructed by the integrated radar-mote system.

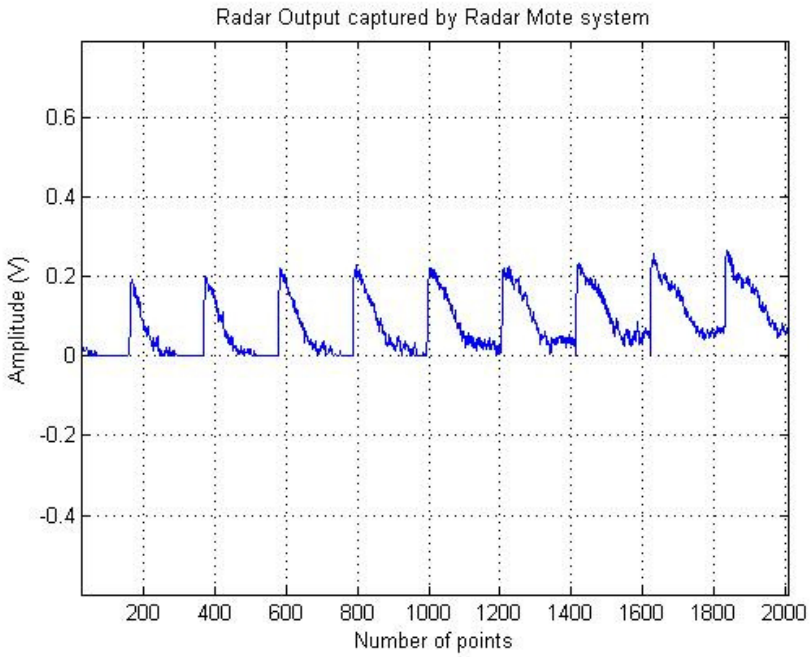

Fig. 23: Radar signal captured and reconstructed using wireless mote

In Fig. 23 the radar signal is captured with a sampling rate of 200 KHz. The signal contains Doppler shift which corresponds target velocity. The signal is checked by processing it through a Matlab program to compute range and velocity of the target. The Matlab program computes a two dimensional FFT of signal and plots them in scaled image with axes corresponding to range and range-rate (velocity).The background for data processing is presented in Chapter 2. The processing of the signal in Fig.39 in Chapter 4 offers approximately correct range and velocity. The detail results for range and velocity computation is discussed in Chapter 4.

3.2 New Doppler model for Reflectivity of non-conducting materials

In Chapter 2, we discussed a mathematical model to shows the amount of reflected electromagnetic energy back to a source from an object. The model

offers the reflection of a plain wave from the object. In this section, we modify the reflection model to incorporate Doppler shift. The signal from new model offers range and velocity information along with the reflectivity of the object. We obtain simulated signal reflected back from a three non-conducting materials using the modified model. The simulated signals are then compared with the experimental signal in Chapter 4.

3.2.1 Modifying the Reflectivity model of Microwave Signal to incorporate Doppler shifts.

The reflectivity model discussed in Chapter 2 offers reflectivity of plane wave from different types of non-conducting surface [7][8]. This section discusses our modifications to the plane wave reflectivity model to incorporate Doppler principle. Adding Doppler shift to plane wave does not change the amplitude of the original signal. However, the added Doppler shift can be used to compute the range and velocity of the target from which the signal is reflected back to the source.

The plane wave model in Eq. (50) can be re-written as follows [8],

$$R = \frac{(1-n_m^2)+(n_m^2-1)e^{i\omega n_m L}}{(n_m+1)^2-(n_m-1)^2 e^{i\omega n_m L}} \quad . \tag{64}$$

Here, $\omega = 4\pi f/c$, c is the speed of light, f is the frequency of the plane wave signal, n_m is the refractive index of the reflecting material and L is the thickness of the reflecting material. The K_a Doppler radar used in our work is dual channel

radar. The two outputs are: In-phase (I) and Quadrature (Q) channel outputs where Q-channel output is 90° phase shifted version of the I-channel radar received signal. The dual channel output can be expressed as,

$$F(t) = I(t) + iQ(t). \tag{65}$$

The details of the Doppler principle are discussed in Chapter 2. We rewrite Eq. (9) for I (t) as follows,

$$I = \frac{\sigma}{2}\cos[4\pi f_0 r/c], \tag{66}$$

where f_0 is the carrier frequency, σ is a constant which corresponds to the target radar cross section (RCS) and $r(t) = r_0 + \dot{r}t$. Note r_0 is range at instant zero and $\dot{r}$ is the rate at which the object is changing its range, range-rate or velocity of the object. The Q-channel signal or Q (t) can be expressed similarly as,

$$Q = \frac{\sigma}{2}\sin[4\pi f_0 r/c]\,. \tag{67}$$

Substituting Eqs. (66) and (67) into Eq.(65) and using well known identity,

$e^{ix} = \cos x + \sin x$, we can write F(t) as,

$$F(t) = \frac{\sigma}{2} e^{\frac{i4\pi f_0 r}{c}}\ , \tag{68}$$

and

$$F(t) \ = \frac{\sigma}{2} e^{i\omega}. \tag{69}$$

Plugging the value of ω from equation (69) to equation (64) we obtain the model of reflectivity that incorporates Doppler shift. The new model equation given is as,

$$R = \frac{(1-n_m^2)+(n_m^2-1)e^{i4\pi f_0 \ r \ n_m L/c}}{(n_m+1)^2-(n_m-1)^2 e^{i4\pi f_0 \ r \ n_m L/c}} \quad . \tag{70}$$

Equation (70) is our final model to obtain the reflectivity of different non-conducting materials in our subsequent integrated Doppler radar-mote integration.

3.2.2 Simulation of Doppler Signal Reflectivity for Non-conducting material surface

The reflective model derived in Eq. (70) assumes the reflective materials are non-conducting and homogeneous. Consequently, we choose a few non-conducting materials for reflectivity simulation. The example materials in our simulation are wood, paper and glass. These materials have their own refractivity defined by index of refraction [8] given as,

$$n = \frac{c}{v} = \frac{\sin\theta_i}{\sin\theta_r} \quad , \tag{71}$$

Here c is the speed of light in vacuum and v is the speed of light in the materials,θ_i is the angle of incidence of wave and θ_i is the angle of reflectance of the wave.

The refractive indexes of the materials depend on the frequency with which it is measured [8]. However, for any material the refractive index is constant for a frequency range. For simplicity we vary the index of refraction for the three materials in our experiment keeping the frequency range same as our Doppler radar. Therefore, the simulated signal will represent the reflectivity of Doppler signals from those material surfaces. Typical refractive indexes of wood, commonly used glass and paper are shown in Table 4.

Table 4: Typical Index of refraction for non-conducting materials used in simulation. (Source: Ref. [7][8])

Materials	Index of Refraction
Wood	1.41
Glass	1.51
Paper	1.73

Figure 24 shows the simulated reflectivity of Doppler radar signal for wood, glass, and paper respectively.

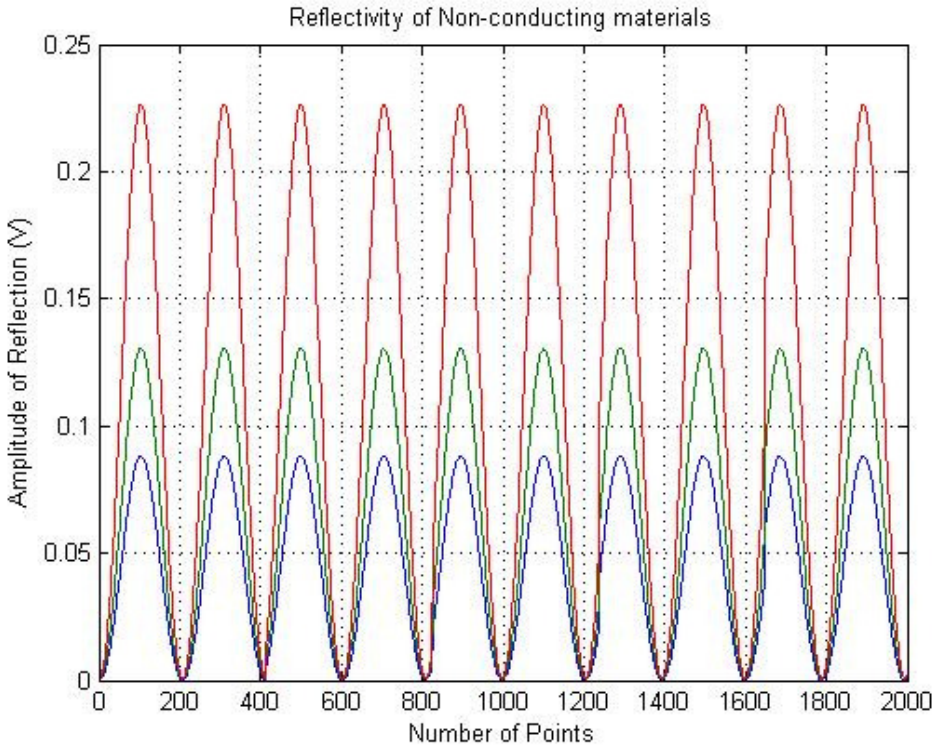

Fig. 24: Reflected Doppler radar signal from non-conducting materials

Figure 24 confirms that our reflectivity model correctly obtains increased reflectivity for objects with higher refractive indices.

3.3 Feature Extraction and Classification of Materials using MUSIC Technique

From the simulation plot in Fig. 24 in section 3.2.2 it is obvious that different types of materials reflect different amounts of energy. In order to obtain a more quantitative measure of this observation, we now design experiments. The simple way to validate the observation is to compare the simulated signal with experimental signal. However, for large amounts of data this simple process may

not be feasible. The data collected through experiment will be too large to validate with visual observation. Therefore, we need to extract feature for each cases and classify them with standard machine learning techniques. Figure 25 shows the machine learning technique we use for the classification.

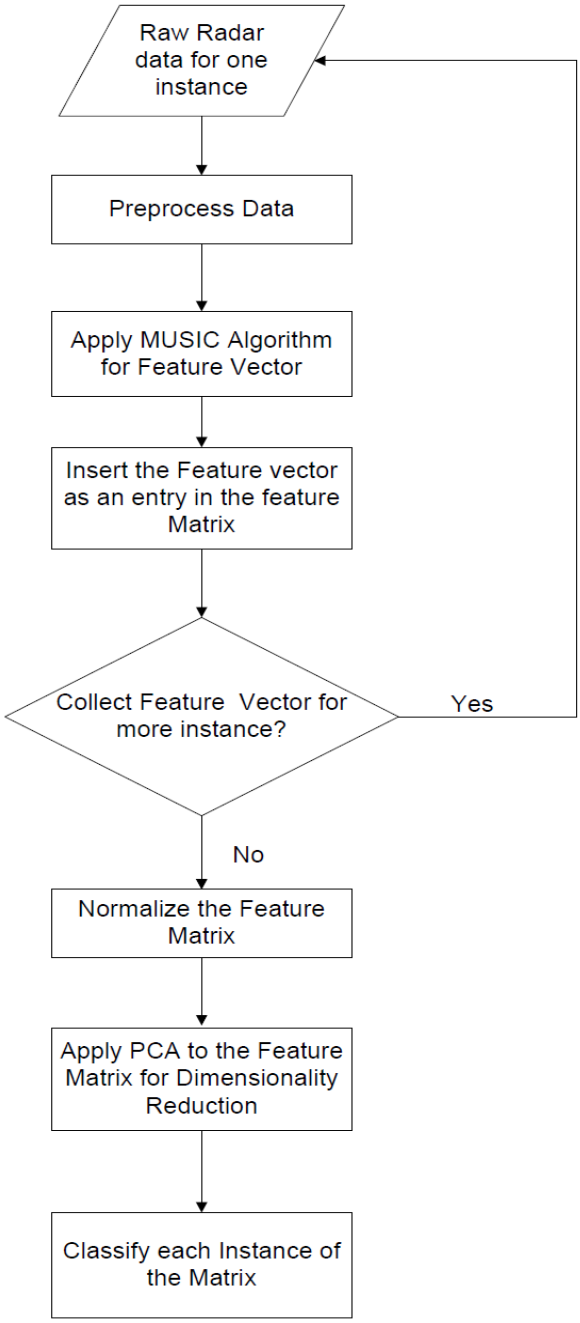

Fig. 25: Methods of Feature Extraction and Classification

We propose a step by step validation process which offers classification matrix as an end result. For feature extraction we use the standard MUltiple SIgnal Classification (MUSIC) technique for spectrum analysis of signal. The detail of the MUSIC technique is discussed in Chapter 2. We have collected data using integrated radar-mote for many instances. The details of the experiment scenario and process are described in Chapter 4. After extracting we apply standard machine learning techniques to classify signals reflected from different material surfaces. We use WEKA machine learning tool for the classification steps [38]. The results of experiments are also discussed in Chapter 4. The detail steps for feature extraction and classification are shown in Fig.25.

For robust object material classification, we need to collect Doppler radar signal reflected from the surface of non-conducting materials for many runs. Each instance of the Doppler signal reflected back from a material surface is treated as one run. The data collected through the integrated radar-mote system is treated as raw data. The raw data is preprocessed by removing any outlier noise and subtracting the background of the signal. We apply the MUSIC technique to the preprocessed signal for extracting features. Similarly, we collect feature vectors for the desired number of runs for all the non-conducting materials and label them for classification. After collecting feature vectors from available number of runs, we normalize the matrix with its maximum value. We then apply Principal Component Analysis (PCA) to reduce the dimensionality of the feature matrix. Finally, we apply different individual classifier and their fusion available in WEKA

to classify them according to the labels assigned. The classification result is discussed in Chapter 4.

In this chapter we discussed our new radar-mote design and implementation. We also discussed corresponding data collection for the verification of our design and testing of the new sensor-mote system. After successful verification of our integrated radar-mote system we design a toy experimental scenario for surveillance and tracking using our novel radar-mote system in Chapter 4. In Chapter 4, we describe the real experiment performed with the integrated autonomous radar-mote system and corresponding results. We further discuss our modification to the reflectivity model [7][8] to incorporate Doppler shift. Both simulated and experimental reflectivity of some non-conducting materials is presented. Finally, a classification technique is proposed to classify the reflectivity of those non-conducting materials to confirm the simulation observation in Chapter 4.

Chapter 4

Experiments and Results

In previous chapters, we introduced an autonomous wireless sensor network consisting of several COTS sensors including Doppler radar, infrared, acoustic and vibration. Such sensor network platform can be used for an integrated surveillance and sensing system [1]. We also designed a toy experiment to explore the capability of our integrated radar mote. In this Chapter, we describe the simulation results of the reflectivity of non-conducting material, the toy experiment, and data collection using the integrated radar-mote sensor network and data processing results. The data collected from toy experiment are compared with the simulated reflectivity of non-conducting materials to validate the idea of different reflectivity for different non-conducting materials. We process the data with simple signal processing technique to compute the range velocity of the targets. We also extract feature from radar signals reflected from non-conducting reflectors with the help of MUSIC technique described earlier. We demonstrate the detection, ranging and velocity estimation with our integrated radar-mote sensor suite and compare the results with that of the radar before integration. We then classify different types of non-conducting materials exploiting extracted features from the Doppler data. The results demonstrate that cheap COTS sensor may be useful to implement effective distributed intelligent decision support system.

4.1 Simulation Results on Reflectivity for selected non-conducting materials

In Chapter 3, we discuss a mathematical model to relate the refractive index of a material and amount of reflected electromagnetic energy from such material. We also discuss our modification to the model incorporating Doppler shift into the electromagnetic wave equations as shown in Eq. (70). The simulation model in Eq. (70) offers synthetic reflected signal for various reflectors made of different materials. Appropriate signal processing of simulated signal is expected to offer range between the reflector and the source as well as the velocity of the moving reflector target. The refractive index of the non-conducting materials used in simulation is shown in Table 4 in Chapter 3. We plot the amplitude of reflected electromagnetic signals for wood, glass and paper reflector respectively in Fig.24 in Chapter 3.

4.2 Range-Velocity Output from Simulated signal

Since we add Doppler shift to our reflectivity model, the simulated signal now shows the range and velocity of the target material along with reflectivity. Figures 26 and 27 show the plot of velocity vs. range of the simulated signal for wood for an example. Note the Doppler shift is not related to amplitude of the reflected signal. Hence, we obtain same plot for all three materials in our experiment. We perform Fast Fourier Transforms (FFT) of the simulated signal and obtain corresponding range and velocity plots. The distance between the moving target and the source of the signal is 0.5m and 1 m respectively in Figs.26 and 27 and

the velocity of the moving reflector is 0.5m/sec for both cases. Since the Doppler shift expression in Eq.70 is same for all the reflectors, we show the corresponding plots for one example reflector (wood) in here.

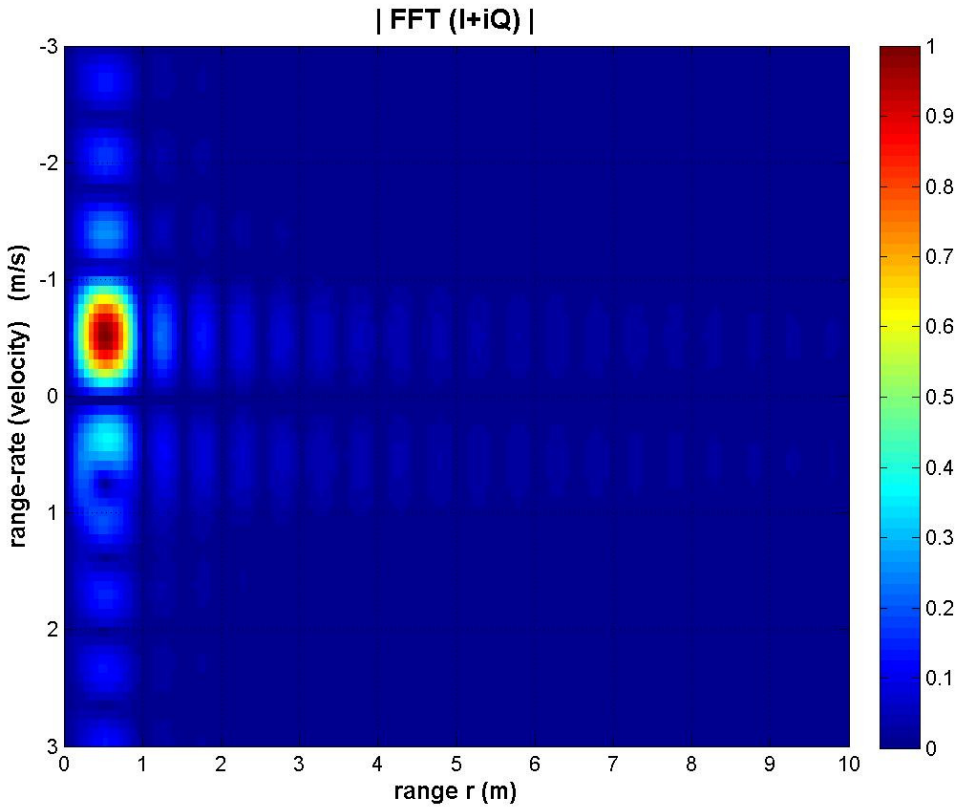

Fig. 26: Range-rate (Velocity) vs. Range plot of simulated signal when the distance between the reflector (wood) and the source of signal was 0.5m and the velocity of the target was 0.5m/sec.

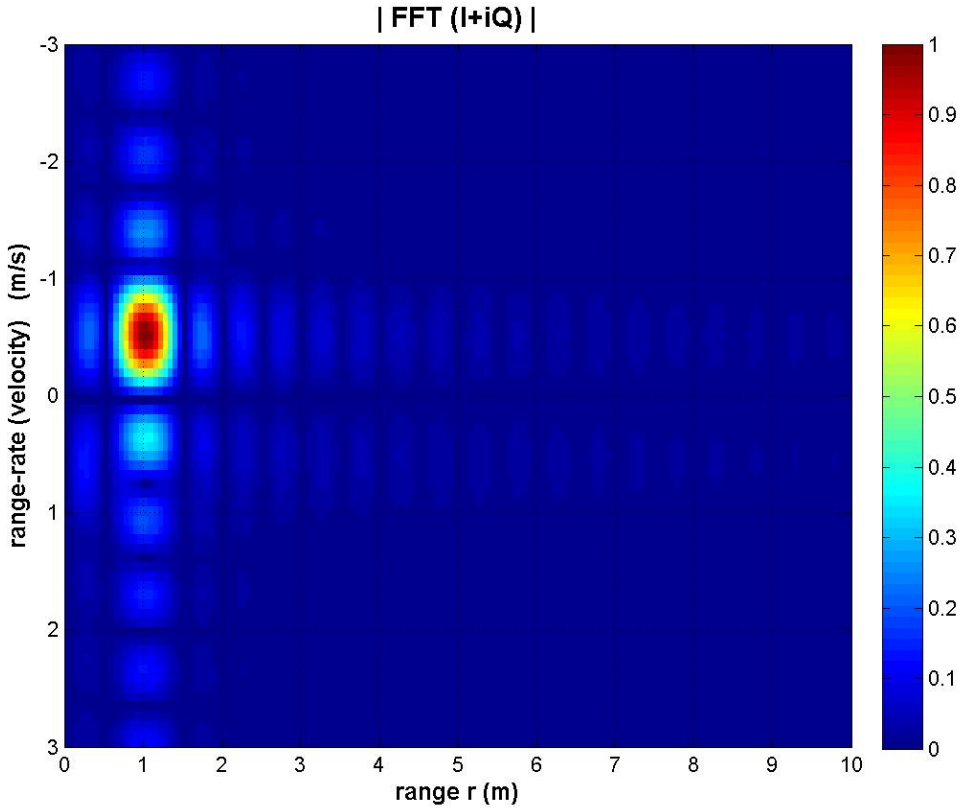

Fig. 27: Range-rate (Velocity) vs. Range plot of simulated signal when the distance between the reflector (wood) and the source of signal was 0.5m and the velocity of the target was 0.5m/sec.

The simulated velocity vs. range offers the same known velocity vs. range measures for our experiments. Therefore, the plots in Figs.26 and 27 show that our modification has successfully incorporated the Doppler shift into the new reflectivity model. We also collect radar signals reflected from the same materials used in this simulation experimentally for comparison and verification.

4.3 Experimental setup for Sensor Network

In this section we discuss the experimental setup and different experiment scenarios using our integrated radar-mote system. Detailed descriptions of the sensors, sensor nodes and integration are discussed in Chapter 2 and 3. We use a toy train as our target. The train is run by battery power and moves round an oval shape track. We emulate different events by making changes to the toy train configurations. Figure 28 shows the experimental sensor network setup with a toy train on the track.

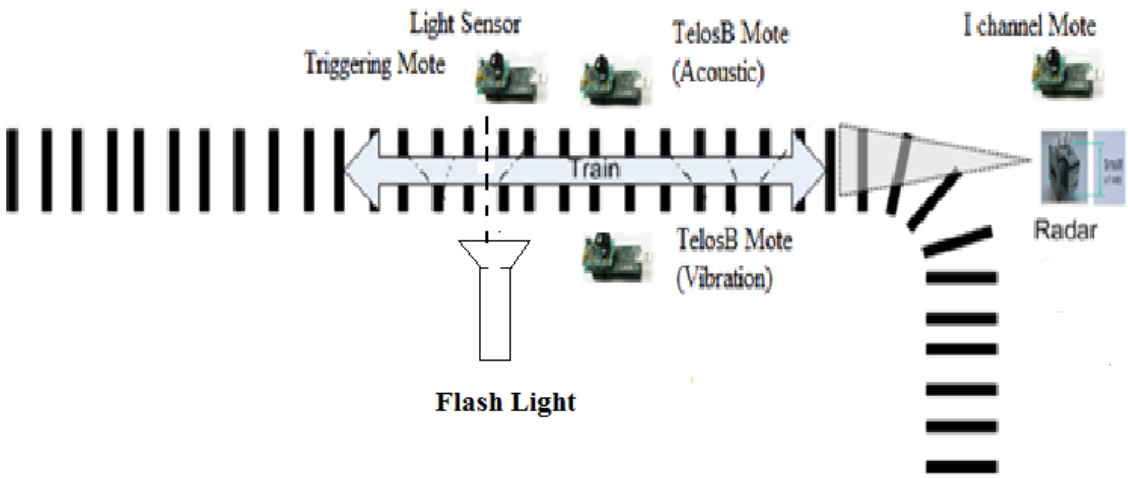

Fig. 28: Experimental set up of our autonomous distributed sensor network which includes integrated radar-mote, SBT80 sensor mote, and WiEye sensor mote.

The WiEye sensor platform has a number of sensors such as passive infrared, visual light and acoustic. The visual light sensor can detect the presence or

absence of light. We use WiEye wireless mote with light sensor as a “sentry” node which detects presence of a moving target and activate the radar-mote system collecting data. The other sensors in WiEye are not used in this experiment. We use these raw signals for computing range and velocity of the toy train and classifying the different materials the radar reflector is made of with the help of simple signal processing and classification algorithm. Figure 29 shows the picture of the integrated radar-mote setup during experiment. Figure 30 shows another picture which includes the moving toy train on the track and the radar-mote sensor system.

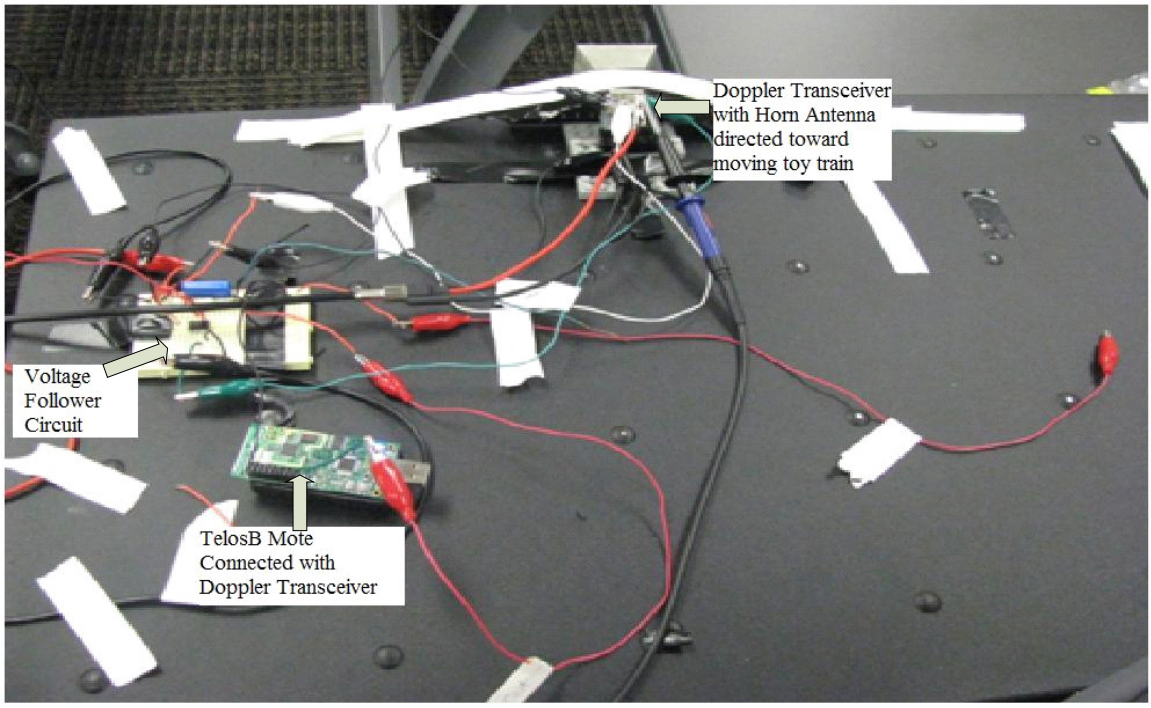

Fig. 29: Picture of the integrated radar-mote setup during experiment.

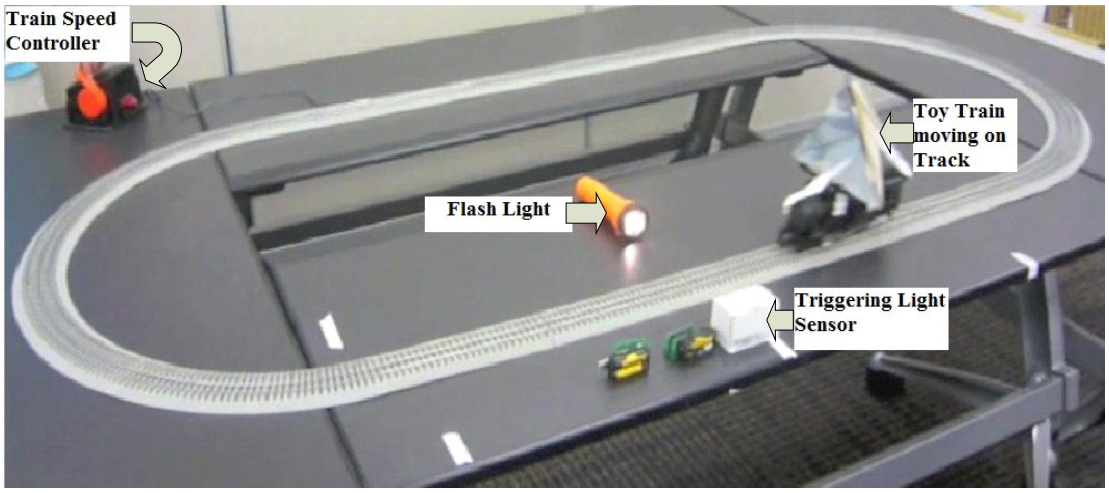

Fig. 30: Picture of the Experimental scenario where toy train is moving on a track.

For testing, we create three different types of reflection profiles with three non-conducting materials such as wood, glass and paper (same materials used in simulation) of the train. We place these different reflection materials at the front of the train such that the directed beam of radar signal is reflected back from these reflection plates. The same setup is used for two different speeds of the toy train. In first case the train moves towards the radar and in the second case, the train is moves away from the radar. The speed of the train is slightly different for two cases. The movement of the target in different direction compared to the static radar may cause different types of incident angle for reflection of the electromagnetic signal. Therefore, we collect the radar data for two different speeds and two different distances. Table 5 summarizes different test events for our toy train.

Table 5: Different Test Configuration created with toy train

Configuration	Type	Description	Remarks
Reflector	Wood, Glass, Paper,	The front of the train holds a rectangular plate that works as a reflector. The reflector is made of the non-conducting materials (wood, glass, paper) and aluminium for different cases.	Due to different material properties we expect difference in amplitude of the reflected radar signal.
Range	0.5m,1m	The distance between the moving target and the static radar is 0.5m and 1m for two different configuration	Different distances between the static radar and moving target is computed from the simulated and experimental signals.
Velocity	Slow and fast	The train has slightly different velocities while moving forward and away from the target.	Different direction of the movement compared to the static radar create slightly different incident angle for the radar signals.

4.4 Experimental Results on Reflectivity for selected non-conducting materials

The simulated signal reflected from three non-conducting materials are discussed in section 4.2. In this section, we collect the corresponding experimental radar signal reflected back from rectangular reflective plate made of the same non-conducting materials respectively. Although the reflectivity model

we use does not work for conducting materials such as metal, we collect reflection data with a metal (tin) reflector as a test case. Figures 31, 32, 33, and 34 show experimental signals reflected back from the same three non-conducting materials and a metal reflector made of wood, glass, paper and tin respectively.

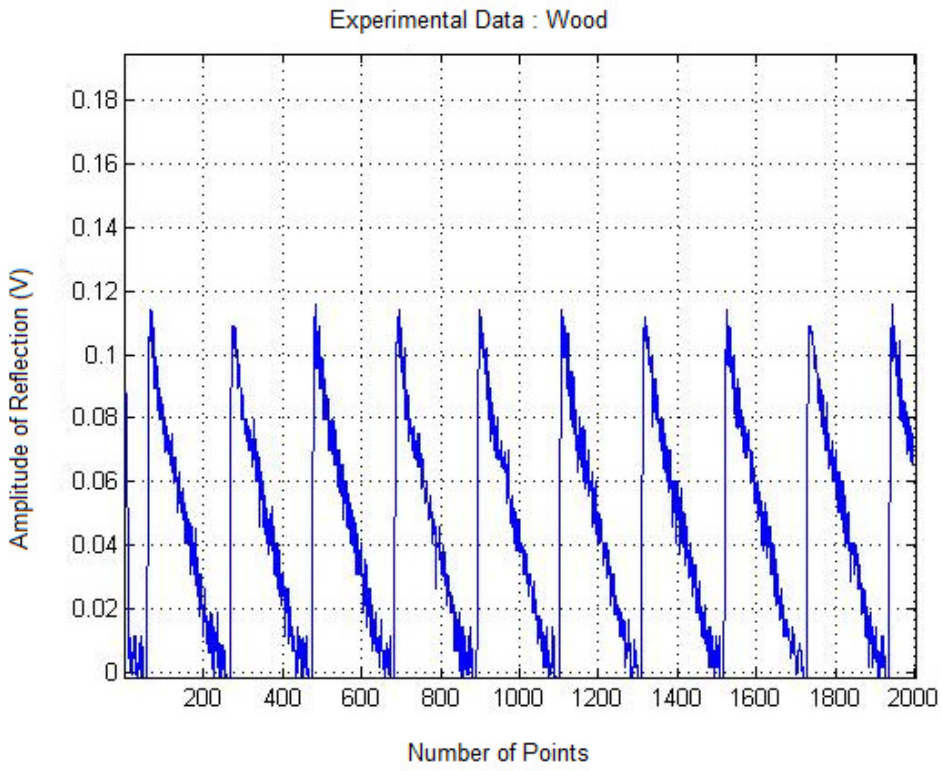

Fig. 31: Experimental Signal Reflected back from Wood

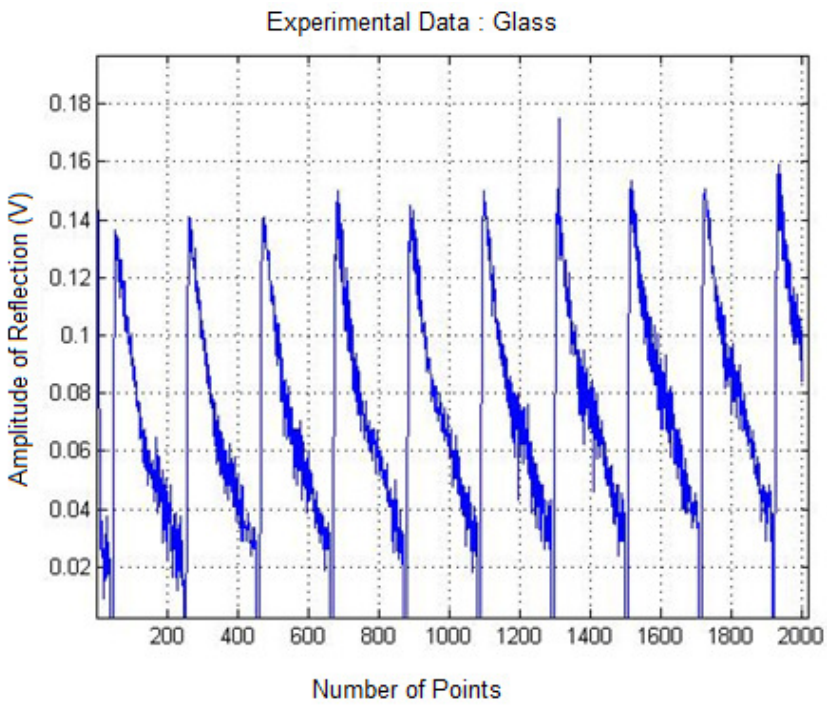

Fig. 32: Experimental Signal Reflected back from Glass

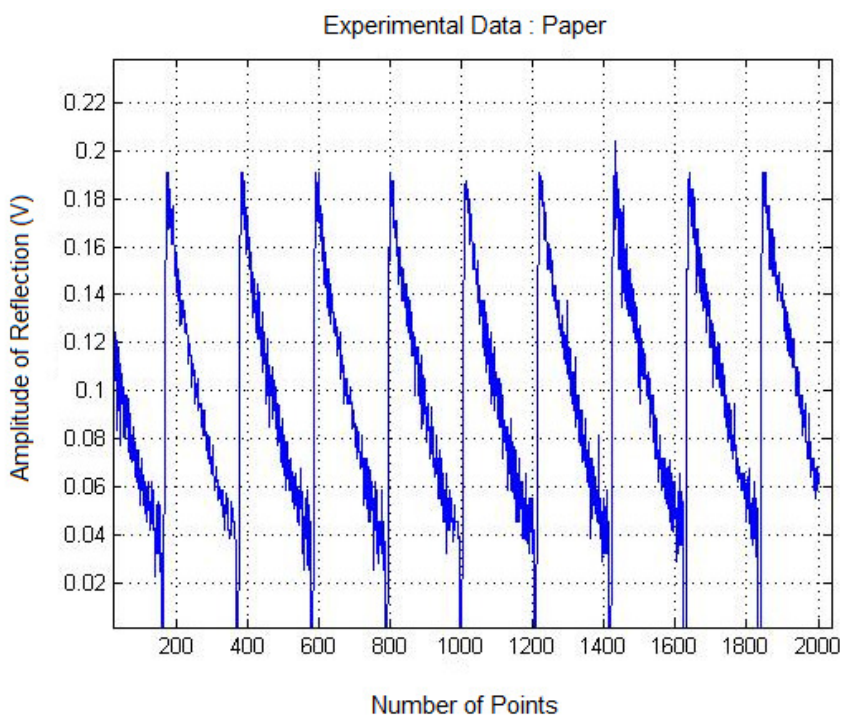

Fig. 33: Experimental Signal Reflected back from Paper

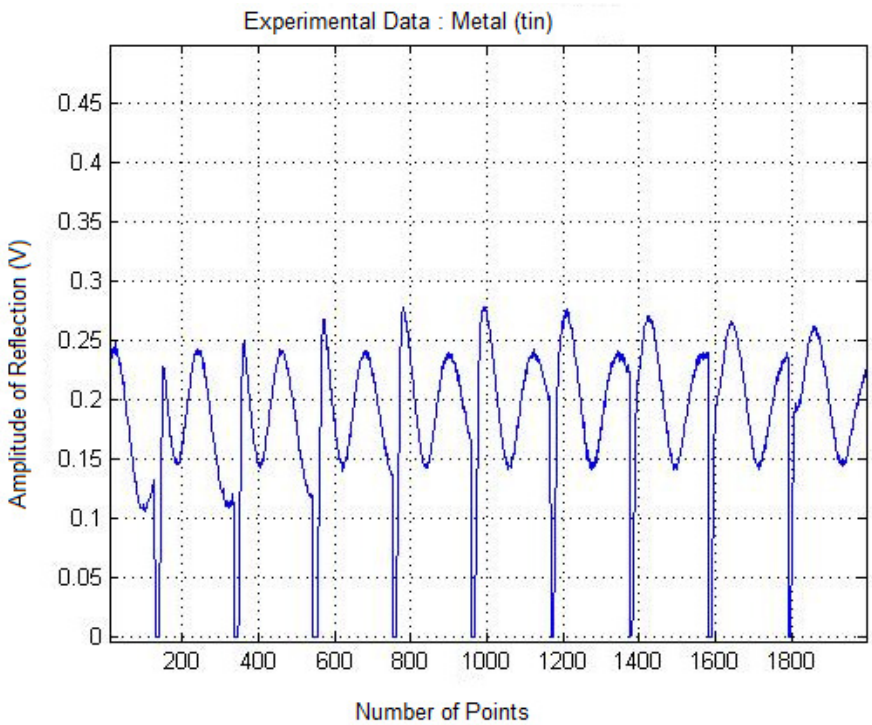

Fig. 34: Experimental Signal Reflected back from Metal (Tin)

The experimental signals in Figs. 31, 32, and 33 are very similar to the simulated signals in Figs 24 for magnitude values. Since the simulated model is a simplified case of reflectivity computation, the slight difference between simulation and experiment is expected. However, the common pattern of amplitude is consistent in both simulation and experiment results. The metal works as a better reflector of the radar signal than the non-conducting materials as shown in Fig.34. Note the experiment conditions are designed to match the simulation as much as possible. The results show that the reflectivity of the materials is an important factor which influences how much energy reflects back to source from a materials surface.

The phase of the signals reflected back from the same three non-conducting reflectors are expected to be similar since the shape of the reflectors is same for all three cases. We present the frequency vs. phase plot of the signals reflected back three non-conducting reflectors in Figs. 35, 36 and 37 respectively. Although the phase plots are almost similar, there is a slight shift in frequency. The moment the radar-mote starts sampling a signal it can be at any point of a ramp like wave. Therefore, we try to align all the radar signals before further processing. However, this alignment process is not perfect .Therefore, the slight shift may occur in different signals. We try to trigger the mote at the same distance for all the experimental cases. However, the response time of the mote may slightly vary for different cases as they are not collected simultaneously. This may cause slight delay between different signals as well.

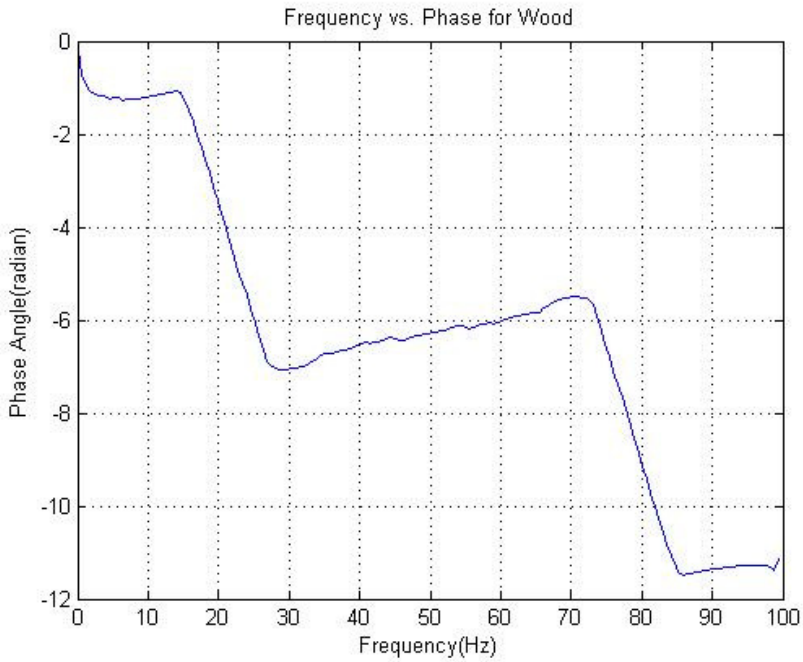

Fig. 35: Frequency vs. Phase Angle plot of the experimental Signal Reflected back from wood

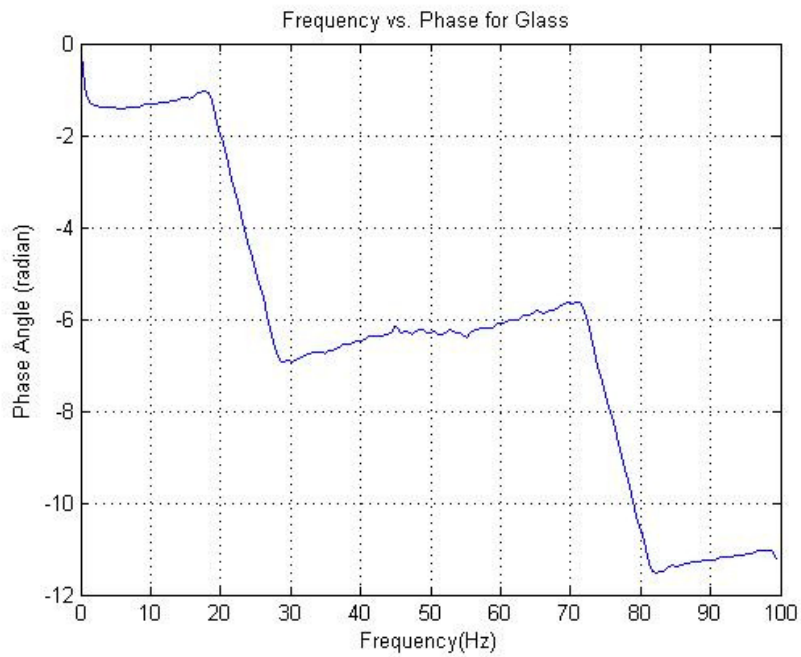

Fig. 36: Frequency vs. Phase Angle plot of the experimental Signal Reflected back from Glass

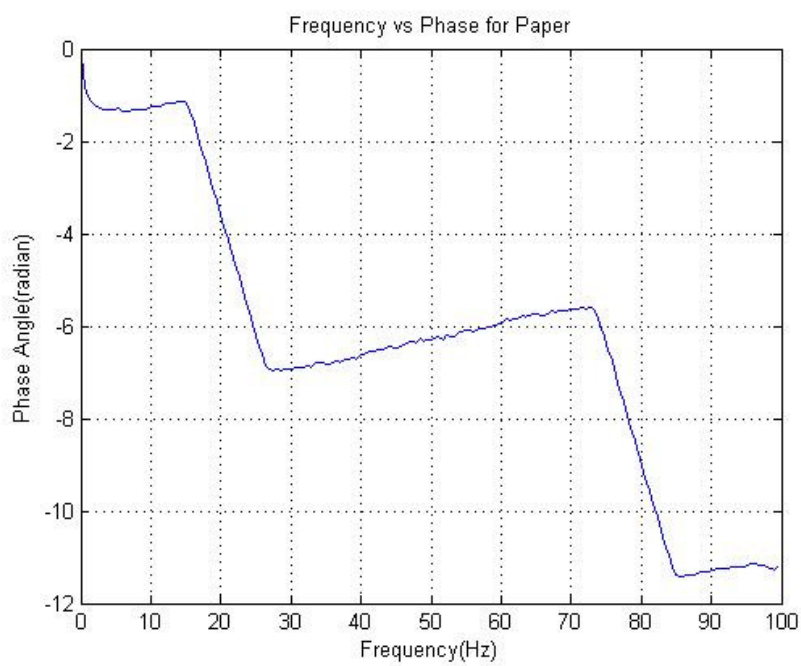

Fig. 37: Frequency vs. Phase Angle plot of the experimental Signal Reflected back from Paper

Figures 35, 36, and 37 demonstrate that there are slight discontinuities in phase plots. These artifacts may occur from quantization error of the ADC or the wireless mote. The comparisons between simulated and experimental results shown in Figs. 24, 31, 32, and 33 is feasible for only a small number of examples. However, to confirm whether same observation is consistently correct, we need to validate our results using large amounts of data. We collect data for many instances for all three non-conducting materials and classify data using the tools discussed in Chapters 2 and 3. The next section discusses our classification results for non-conducting materials. The steps starting from data preprocessing to classification are shown in a flow chart in Fig. 23 in Chapter 3.

4.5 Range-Velocity Output from Experimental Signal

The Doppler radar is expected to offer range-velocity as output. The range-velocity output from simulated signal is shown in Figs. 26 and 27 for distances of 0.5 m and 1m respectively. Now we process the radar data collected from the integrated radar-mote. We compare these range-velocity plots with the plots of standalone radar data. Figures 38 and 39 show the range-rate (velocity) vs. range plots using the data captured through newly designed integrated radar-mote system. Figure 38 shows the range-velocity plot when the toy train moves toward with a velocity of 0.5m/sec and the distance between the target and radar-mote is 0.5m.Similarly; Fig.39 shows the range-velocity plot when the toy train moves toward with a velocity of 0.5m/sec and the distance between the target and radar-mote is 1m.

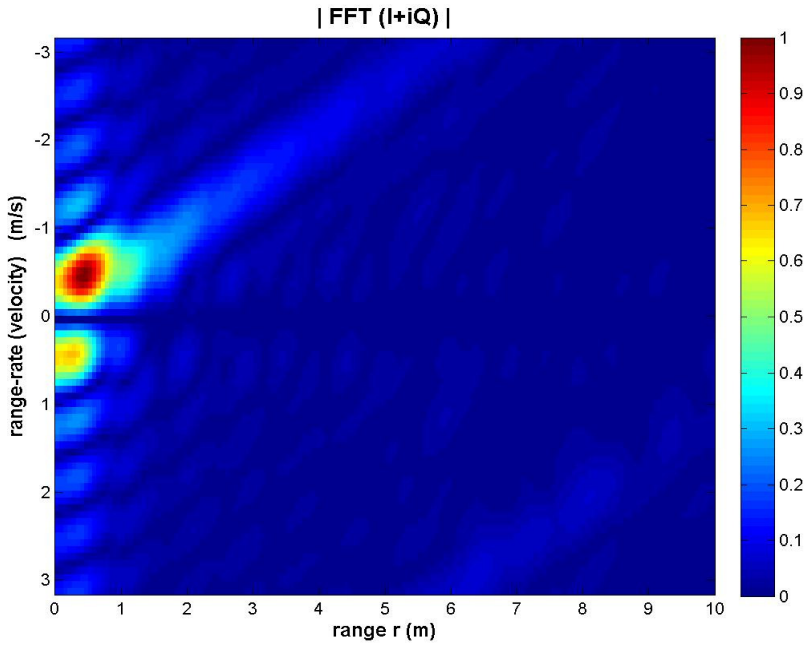

Fig. 38: Range-rate vs. Range plot when the toy train was moving toward the radar and the data is captured through radar-mote (range 0.5m and velocity was 0.5m/sec).

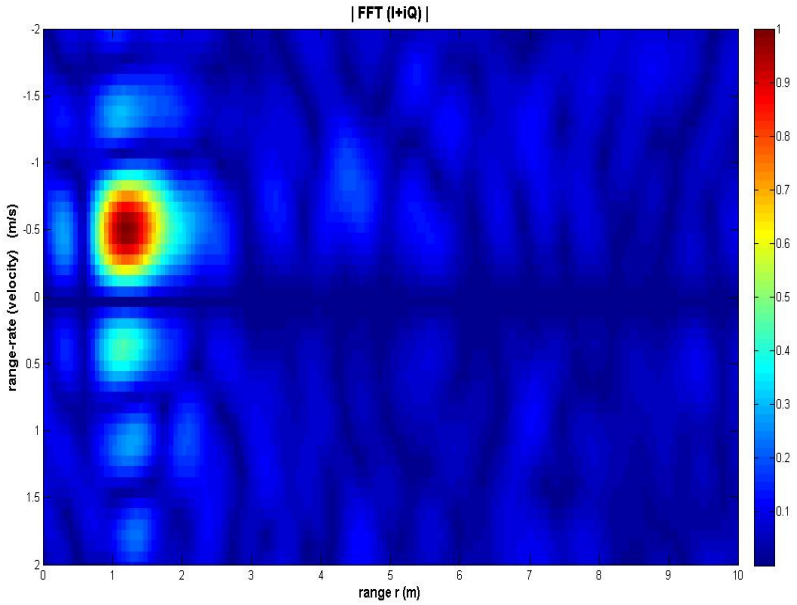

Fig. 39: Range-rate vs. Range plot when the toy train was moving toward the

Radar and the data is captured through radar-mote (range 1m and velocity 0.5m/sec).

For cross check and validation, we collect data for same configuration using stand alone radar system with the help of a storage oscilloscope. Now we present the plots for same configurations as the radar-mote plots. Our troy train moves toward the radar with velocity 0.5m/sec and the distances are 0.5 m and 1 m respectively for two cases. Figure 40 shows the range-velocity plot when the toy train was moving toward with a velocity of 0.5m/sec and the distance between the target and radar-mote is 0.5m. In Fig. 41 all the configurations are the same as in Fig.40 except the distance between stand-alone radar and target is 1 m.

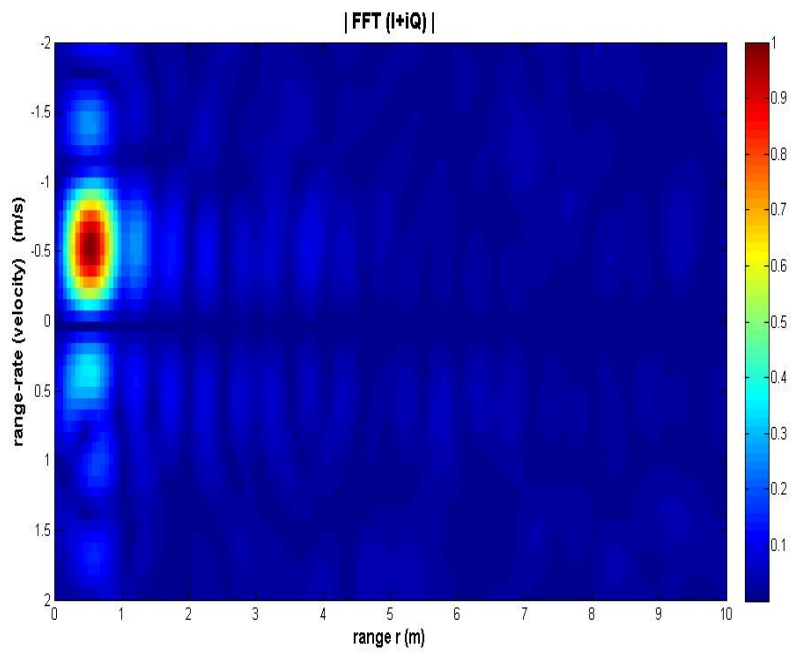

Fig. 40: Range-rate vs. Range plot when the toy train was moving toward the radar and the data is captured through storage oscilloscope (range 0.5m and velocity is also 0.5m/sec).

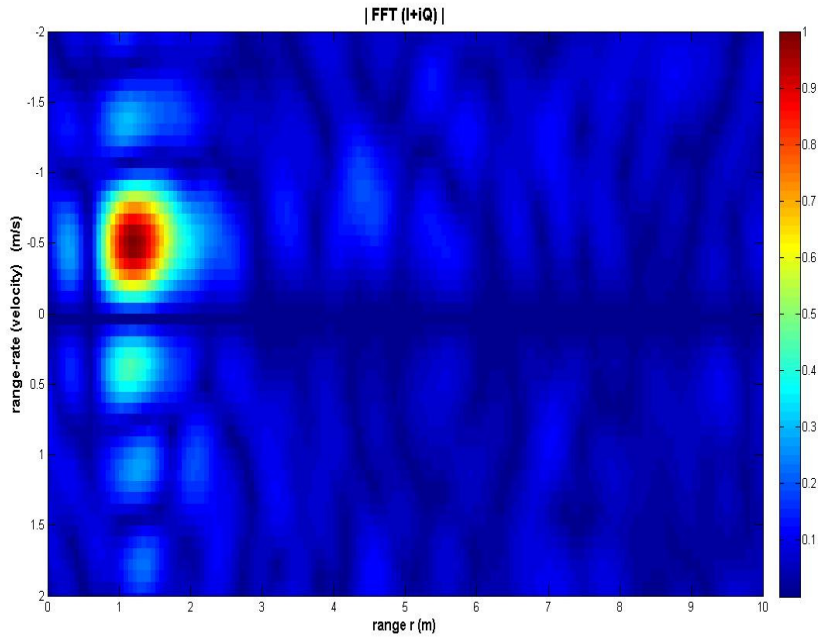

Fig. 41: Range-rate vs. Range plot when the toy train was moving toward the radar and the data is captured through storage oscilloscope (range 1m).

Comparing the plots in Figs. 38 and 39 to those in Figs.40 and 41 for same configuration for our integrated radar-mote confirms validation of our novel radar-mote system.

4.6 Classification Results for non-conducting materials

One of the goals of this thesis is to explore whether we can use material properties, specifically refractive index of materials, to classify the materials types of the targets. For simplicity and limited scope of this thesis, we obtain a modified model for non-conducting materials as shown in Eq. (70). We collect reflected radar signal from three non-conducting materials such as wood, glass and paper with our integrated radar-mote autonomous system. The pseudo- spectrum of the

signal, computed with MUSIC algorithm, is selected as the feature to classify the non-conducting material types of the target.

We provide a brief description of the classification process here. Each instance of the radar signal is treated as one run and we collect 30 instances for all three non-conducting reflecting materials for each configuration. We take the raw signal for each instance and perform preprocessing. The MUSIC technique is then applied to the signal to obtain feature vector for that instance following the steps shown in Fig. 25. Note, the machine learning techniques and WEKA toolbox are discussed in section 2.7 in Chapter 2. Table 6 shows the result of classification using different types of classifier for the three non-conducting materials.

Table 6: Result of classification with Weka Machine Learning Tool

Class	Description of runs	Test Training Split	Total # of runs	Classifier	Accuracy %	True +ve Rate	False +ve Rate	[1]ROC Area	[2]Kappa Statistic
Glass, Paper, Wood	2 velocities (Train moving forward and train moving backward) and 2 distances (50cm, 100cm)	10 fold cross validation (66% for training and 34% for testing)	359	J48 (A decision tree based classifier)	79.94	0.79	0.1	0.87	0.70
			359	Support Vector Machine1	95.26	0.95	0.024	0.96	0.93
			359	Support Vector Machine2	92.75	0.92	0.036	0.95	0.89
			359	LMT: Logistic Model Trees (Decision tree based	89.69	0.89	0.052	0.95	0.84

				on logistic regression)					
			359	Random Forest (A tree based classifier)	90.52	0.90	0.047	0.98	0.86
			359	Multi Layer Perceptro n (MLP)	91.64	0.91	0.042	0.98	0.87
			359	Rotation Forest (A meta classifier that uses a base classifier)	90.52	0.90	0.047	0.99	0.86
			359	Voting of Random Forest, LMT and MLP	94.98	0.95	0.025	0.99	0.92
			359	Voting of Random Forest, Rotation Forest and MLP	94.98	0.95	0.025	0.99	0.92
			359	Voting of Random Forest, Rotation Forest and LMT	92.20	0.92	0.039	0.99	0.88
			359	Voting of Random Forest, SVM and LMT	96.10	0.96	0.019	0.99	0.94
			359	Voting of Random Forest, SVM and MLP	95.82	0.95	0.021	0.99	0.94

In Table 6, we use the following classifiers J48, functional tree, logistic model tree (LMT), random forest, rotation forest, multilayer Perceptron (MLP), support

vector machine (SVM) and fusion of a few better performing classifiers. We fuse the classifiers using the meta classifier in WEKA toolbox based on voting of the classifiers. Table 6 shows that Support Vector Machine and Multilayer. Perceptron classifiers provide the highest percentage of accuracy when individually compared to the other classifiers. The fusion of four combinations of different classifiers such as random forest-SVM-MLP, random forest-SVM-LMT, random forest-rotation forest-LMT and random forest-LMT-MLP provide more accuracy compared to any of the individual classifiers. The classifier accuracy is close to 90% for most of the classifiers. The area under ROC overall, which is another test of accuracy, is also close to 0.9 in scale of 1.0 for most of the cases. The figs. 42, 43 and 44 reflects this statement about ROC also. We show the ROC plot for one of the fusion classifiers for all three classes wood, glass and paper in Figs.42, 43, and 44 respectively as an example. The Kappa statistic is a measure of the stability for machine learning applications. If the Kappa statistic value is greater than 0.6, it indicates substantial agreement for the classification result [53]. For most of the classifiers in Table 6 the Kappa statistic is above 0.8. Therefore, the classification results are substantially stable.

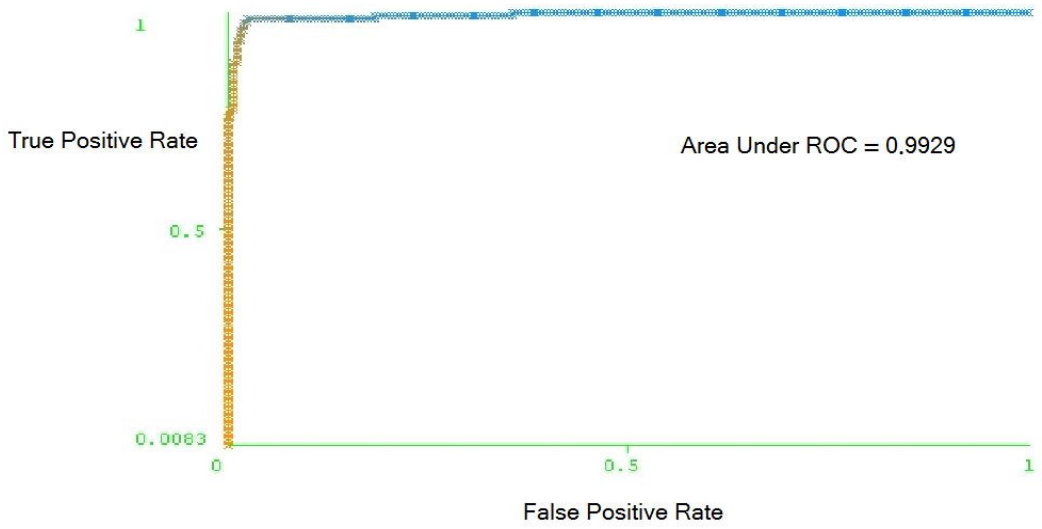

Fig. 42: The ROC curve plot for Fusion of Random Forest-SVM-MLP classifiers for the class wood. The x-axis and y-axis denote the False Positive rate and the true positive rate respectively.

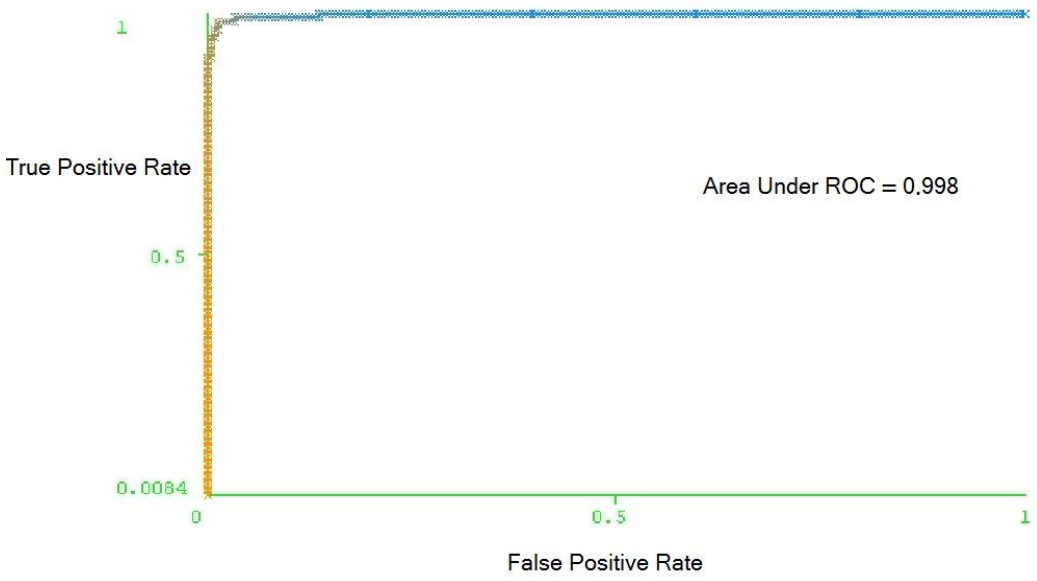

Fig. 43: The ROC curve plot for Fusion of Random Forest-SVM-MLP classifiers for the class glass. The x-axis and y-axis denote the False Positive rate and the true positive rate respectively.

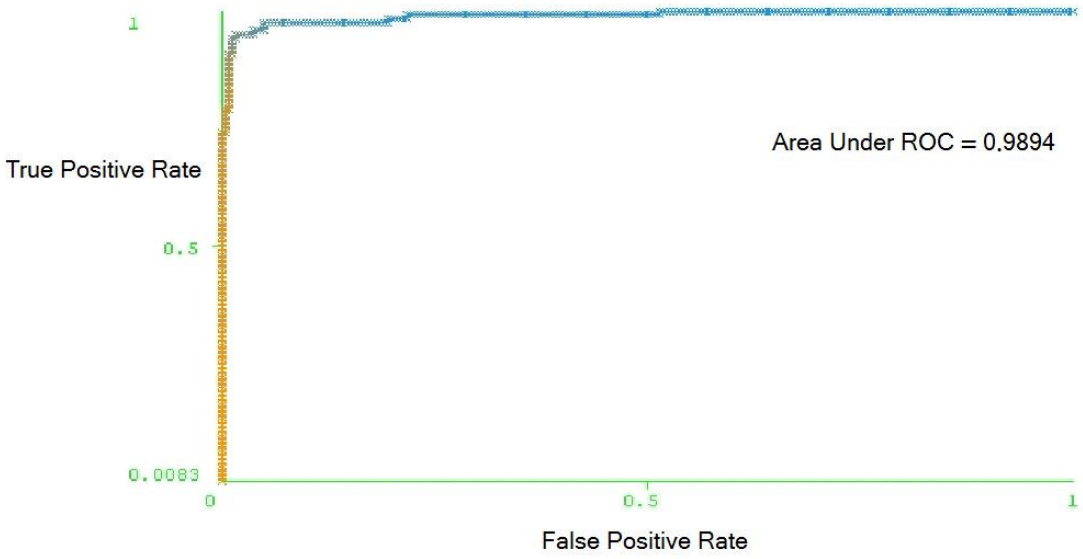

Fig. 44: The ROC curve plot for Fusion of Random Forest-SVM-MLP classifiers for the class paper. The x-axis and y-axis denote the False Positive rate and the true positive rate respectively.

From above discussion and the classification Table 6, we conclude that the materials property can be used as good feature to classify the target material type.

4.7 Advantages of the integrated radar-mote system compared to the standalone Radar system

The aim of our thesis is to integrate a powerful active sensor such as Doppler radar into wireless sensor mote without degrading the capabilities of the standalone sensor systems. Table 7 shows a summary comparison between an integrated radar-mote system versus standalone radar system.

Table 7: Comparison between Standalone Radar and Integrated Radar-Mote system

Features	Standalone Doppler Radar	Integrated Radar-Mote System	Description
Automated Data Collection	No	Yes	The standalone radar system usually needs human intervention to store data in the storage system. Some current digital oscilloscopes may have the software control over the data gathering. However, triggering the digital scope requires complex circuitry and system to operate. Whereas in the integrated Radar-Mote system data gathering system is automated with the help of the wireless network framework of the wireless motes.
Event Driven	No	Yes	The data capturing is triggered when the integrate Radar-Mote gets a triggering signal from a sentry node. In our case the WiEye sensor mote sends the triggering signal when it detects the presence of any object within its field of view. Similar ways using the other sensors available in the wireless node different triggering events can be designed. Whereas the data

			capturing is not event driven in case of the standalone radar system.
Large-scale data collection	Not suitable	Suitable	In case of the stand alone system requires human intervention and the storage oscilloscope also takes at least 5 seconds to store the data at any instant. Therefore, the standalone system is not suitable for large scale data collection where one need to collect many instances of a repeatable event.
Portability and Mobility	Not easily portable and not suitable for remote operation.	Yes	Need large supporting systems like oscilloscope, signal generator and power supply. Therefore, the standalone system cannot be deployed at any place due to specific requirements of the supporting equipments. Whereas the storage oscilloscope is replaced with the tiny wireless mote in the integrated system and the motes are run by battery power. The work is going on to replace the signal generator and power source equipments with the onboard signal generator and power source circuit. That would make the integrated system fully portable and mobile

Remote operation	Not suitable	Suitable	The integrated system can be triggered by the sentry nodes from a distant place through wireless communication. Similarly the base station node which works as bridge between the integrated system and a workstation can also be placed distant place from the integrated radar-mote.
Power requirement	High	Low	The wireless mote which replaces the storage oscilloscope is run by 3 battery power. Whereas the scope requires high power source to operate.

Therefore, we conclude that our integrated radar-mote design and implementation met all goals stated at the beginning of this thesis. Furthermore, we successfully exploit novel integrated radar-mote system for experimental verification of target material classification.

Chapter 5

Conclusion and Future Work

Our contribution in this thesis can be divided into two parts. The first contribution is a successful design and implementation of an integrated autonomous radar-mote system. The second contribution involves experimentation and simulation of reflectivity of non-conducting materials. We have modified an analytical reflectivity model [7] [8] to incorporate Doppler shift. We obtain simulated Doppler signal for various non-conducting materials. Finally, we experimentally verify and classify the non-conducting material targets using real data collected with our newly designed radar-mote system. The following sections elaborate on the contributions of this thesis. We also discuss the limitations and potential future works.

The first goal of the thesis is to incorporate an active sensor such radar into the wireless mote. We successfully design and implement an autonomous radar-mote system integrating a K_a- band Doppler radar to TelosB wireless mote. Our integrated radar-mote system can successfully replicate the data collection capabilities of a standalone radar system. The additional benefits of our integrated radar-mote system include increased automation, large-scale data collection, portability, remote operation and reduced power requirement. Comparing the processed signal collected through radar-mote with that of storage oscilloscope, we find that our radar-mote can compute range-velocity as correctly as the standalone radar does. We add a voltage follower circuit as an

analog buffer to provide required separation between the Doppler radar output and the TelosB mote in here.

The second part of the thesis propose a modified reflectivity model [7][8] to obtain reflected signals from non-conducting material surfaces. The original model offers the reflectivity of a plane electromagnetic wave from non-conducting materials. We modify the model to incorporate Doppler shift into the reflectivity model such that the signal offers range –velocity information of the target in addition to reflectivity of different target materials. We simulate reflectivity of three non-conducting materials such as wood, glass and paper using our modified reflectivity model. The simulated signal is processed with FFT to compute range and velocity from Doppler shift. The simulation results confirm that the Doppler shift is successfully incorporated into the analytical reflectivity model. We experimentally collect reflected radar signals from the same three non-conducting materials using our newly implemented integrated radar-mote system. The radar-mote autonomously captures large amount of signal for different configurations. Our experimental radar-mote reflection data validates our simulated data for the selected non-conducting materials. Finally, we successfully classify three non-conducting materials using the collected reflectivity signals.

The contributions of this thesis are summarized as follows,

1. This thesis accomplishes a successful design and implementation of an autonomous radar-mote by integrating a Doppler radar into the wireless mote with Commercial off the shelf components.
2. This thesis successfully investigates the effect of material refractive index on the reflectivity of non-conducting materials. A reflectivity model for non-conducting material is successfully modified to incorporate Doppler shift information. The newly built integrated radar mote system is used to collect data for successful validation of the reflectivity model.

Our newly designed and implemented integrated autonomous radar-mote system offers reasonable accuracy and efficiency. However, there is still opportunity of improve the system. Although the signal captured through radar-mote system computes the range-velocity correctly, we observe a slightly upward slope in the radar signal captured through the radar-mote system. We need to investigate the unwanted upward slope in our signal to make the system more efficient. Our radar-mote system is still experimental. Hence, more emphasis was placed on correct function rather than efficiency, mobility, and portability. The voltage tune input to the Doppler radar is currently provided from a standard laboratory signal generator. The 5V power required for the radar and voltage follower circuit is also provided from standard laboratory power supply device. The heavy laboratory equipments used in current setup pose inconveniences such as lack of portability and mobility. We plan to replace the standard laboratory signal generator and power supply equipment with equivalent circuit implementation. Since our current system is experimental, we use laboratory connecting wires for the connections

between Doppler radar, voltage follower circuit and TelosB mote. In addition, the random odd glitches present in some cases in the radar signal may occur due to these unstable connections. Once the experimental system is standardized these connection will be replaced with standardized soldered connections. Implementing the whole experimental radar-mote system in a single IC package would be the final target.

We have performed our experiments in an indoor laboratory environment and indoor environment is always advantageous compared to outdoor. Therefore, in real life scenarios and in complex outdoor environment, the classification accuracy of our system may decrease from the current accuracy level. In this thesis, we explore the simple idea of classifying different non-conducting material reflectors. This work can be extended to explore object detection for different types of conducting as well as non-conducting materials in complex outdoor environment. For the sake of simplicity and limited scope of the thesis, we just consider the reflectivity of the non-conducting materials for our simulation and experiment. Therefore, one of the logical directions of improvement is to integrate the reflectivity of the conducting materials into our model. Successful integration of conducting materials into the model will make the model complete.

Reference

[1] R. Kozma, L. Wang, K. Iftekharuddin, E. McCracken, M. Khan, K. Islam, R. Demirer, Multi-Modal Sensor System Integrating COTS Technology for Surveillance and Tracking, Page 1030-1035, Proceedings of IEEE International Radar Conference, Washington DC, USA,2010.

[2] P. Dutta, A. Arora,S. Bibyk,Towards Radar-Enabled Sensor Networks, ISPN'06, Nashville,Tennessee,USA, April 19-21,2006.

[3] K. R¨omer and F. Mattern, The Design Space of Wireless Sensor Networks, IEEE Wireless Communications, Dec. 2004.

[4] A. Tiwary, P. Ballal, F. Lewis, Energy-efficient wireless sensor network design and implementation for condition-based maintenance,ACM Transactions on Sensor Networks (TOSN),Volume 3 , Issue 1 (March 2007).

[5] T. Haenselmann, Sensornetworks, An FDL'ed Textbook on Sensor Networks.

[6] Obtained from: http://en.wikipedia.org/wiki/Radar

[7] J. Kim, Through-The-Wall Imaging from Electromagnetic scattered field measurements, A thesis for partial fulfillment of MS in Physics from Naval Post Graduate School, March 2007

[8] K. Lee, THz-Imaging Through-The-Wall using the Born and Rytov Approximations, A thesis for partial fulfillment of MS in Physics from Naval Post Graduate School December 2008.

[9] T. McEwen, Ultra-wideband radar motion sensor, Pat. #5361070.

[10] TWR-ISM-002-I Radar: Hardware User's Manual, Advantaca Inc., 2002.

[11] Users Manual for the BumbleBee (Model 0): A Mote-Scale Pulsed Doppler Radar for use in Wireless Sensor Networks, The Samraksh Company.

[12] S. Hadim, N. Mohamed, Middleware: Middleware Challenges and Approaches for Wireless Sensor Networks, IEEE Distributed Systems Online, vol. 7, no. 3, pp. 1, Mar. 2006.

[13] A. Mainwarin, J. Polastre, R. Szewczy, D. Culler, J. Anderson, Wireless Sensor Networks for Habitat Monitoring, WSNA'02, Atlanta, Georgia, USA, September 28, 2002.

[14] Obtained from: www.alertsystems.org

[15] L. Schwiebert, S. Gupta, J. Weinmann, Research Challenges in Wireless Networks of Biomedical Sensors. Mobile Computing and Networking, Pages 151-165, 2001.

[16] N. Xu, A Survey of Sensor Network Applications, Computer Science Department, University of Southern California.

[17] S. Rutledge, The PIC Farm: A Multiprocessor Sensor Board, Lancaster University, UK.

[18] Obtained from: http://en.wikipedia.org/wiki/List_of_wireless_sensor_nodes

[19] Obtained from: http://www.cse.unsw.edu.au/~sensar/hardware/hardware_survey.html

[20] Obtained: TelosB Datasheet, www.xbow.com/Products/Product_pdf_files/Wireless_pdf/

TelosB_Datasheet.pdf

[21] User's Guide for Texas Instrument's MSP 430x1xx family. Obtained: http://focus.ti.com.cn/cn/lit/ug/slau049f/slau049f.pdf

[22] Telos Mote User Guide. Obtained from: www.ece.osu.edu/~bibyk/ee582/telosMote.pdf

[23] Obtained from: http://en.wikipedia.org/wiki/TinyOS

[24] Obtained from: http://en.wikipedia.org/wiki/Doppler_radar

[25] Obtained from: http://en.wikipedia.org/wiki/Doppler_effect

[26] Obtained from: http://en.wikipedia.org/wiki/Radar

[27] Obtained from: http://en.wikipedia.org/wiki/Radar_cross-section

[28] Stereo Voltage Controlled Doppler Transceiver Datasheet. Obtained from: www.macomtech.com/datasheets/MACS-007802-0M1R1V.pdf

[29] R. Deming , Determining Target Range and Velocity using Doppler Radar, FIT-AF Workshop, FIT, University of Memphis, January, 2009.

[30] L. Shen and J. Kong, Applied Electromagnetism, Second Edition, PWS Publishers, Boston, MA (1987).

[31] S. Marple, Digital Spectral Analysis, Englewood Cliffs, NJ, Prentice-Hall, 1987, pp. 373-378.

[32] R. Schmidt, "Multiple Emitter Location and Signal Parameter Estimation," IEEE Trans. Antennas Propagation, Vol. AP-34 (March 1986), pp.276-280.

[33] P. Stoica, and R. Moses, Introduction to Spectral Analysis, Prentice-Hall, Englewood Cliffs, NJ, 1997.

[34] T. Georgio, Signal estimation via selective harmonic amplification: MUSIC, Redux, IEEE Trans. Acoust., Speech Signal Process., 2000, 48(3), pp. 780-190.

[35] Z. Tian, Iterative MUSIC: coherent signal estimation, performance analysis, IEEE Int. Conf. Acoustics, Speech and Signal Processing, May 2002,pp. 3041-3044.

[36] Y. Wei, F. Zenghe, A new method for joint DOA and FOA estimation using MUSIC algorithm, Fourth Int. Conf. Microwave and Millimeter Wave Technology, August 2004,pp 219-222.

[37] M. Secmen, G. Turhan-Sayan, Radar target classification method with reduced aspect dependency and improved noise performance using multiple signal classification algorithm,IET Radar, Sonar and Navigation,2009,vol.3,pp. 583-595.

[38] WEKA User Guide. Obtained from: www.cs.waikato.ac.nz/ml/weka/

[39] R. Bouckaert, E. Frank, M. Hall, R. Kirkby, P. Reutemann, A. Seewald, D. Scuse, WEKA Manual for Version 3.6.2.

[40] I. Witten, E. Frank, Data Mining: Practical Machine Learning Tools and Techniques with Java Implementations, Morgan Kaufmann Publishers, 2000.

[41] A. Roberts, AI32-Guide to WEKA (www.comp.leeds.ac.uk/andyr).

[42] J. Quinlan, C4.5: Programs for Machine Learning. Morgan Kaufmann Publishers, 1993.

[43] Obtained from: http://en.wikipedia.org/wiki/C4.5_algorithm

[44] Obtained: http://en.wikipedia.org/wiki/Support_vector_machine

[45] L. Breiman, Random Forests, Machine Learning, Volume 45 (1), Page 5–32, 2001.

[46] F. Rosenblatt, Principles of Neurodynamics: Perceptrons and the Theory of Brain Mechanisms, Spartan Books, Washington DC, 1961.

[47] S. Haykin, Neural Networks: A Comprehensive Foundation (2 Ed.), Prentice Hall, 1998, ISBN 0132733501.

[48] S. Pal, S. Mitra, Multilayer Perceptron, Fuzzy sets, and Classification, IEEE Transactions on Neural Networks, Vol.3, No.5, Page 683-696, September, 1992.

[49] J. Rodriguez, L. Kuncheva, C. Alonso, Rotation Forest: A new classifier ensemble method, IEEE Transactions on Pattern Analysis and Machine Intelligence, 2006.

[50] L. Kuncheva, Combining Pattern Classifiers: Methods and Algorithms, John Wiley and Sons, Inc, 2004.

[51] WiEye Datasheet, Obtained from: www.easysen.com/support/WiEye/DatasheetWiEye.pdf)

[52] SBT80 Datasheet, Obtained from: (www.easysen.com/support/SBT80v2/DatasheetSBT80v2.pdf)

[53] A. Viera, J. Garrett, Understanding Interobserver Agreement: The Kappa Statistic, Fam Med 2005; 37(5):360-3.